Student thesis series INES nr 409

Mapping tree canopy cover in the semi-arid Sahel using satellite remote sensing and Google Earth imagery

Abdalla Eltayeb A. Mohamed

2016
Department of
Physical Geography and Ecosystem Science
Lund University
Sölvegatan 12
S-223 62 Lund
Sweden

Abdalla Eltayeb A. Mohamed (2016).
Mapping tree canopy cover in the semi-arid Sahel using satellite remote sensing and Google Earth imagery
Master degree thesis, 30 credits in Master of *Geomatics*
Department of Physical Geography and Ecosystem Science, Lund University

Level: Master of Science (MSc)

Course duration: *January* 2016 until *June* 2016

Disclaimer

Mapping tree canopy cover in the semi-arid Sahel using satellite remote sensing and Google Earth imagery

---

Abdalla Eltayeb A. Mohamed

Master thesis, 30 credits, in *Geomatics*

Supervisor: Abdulhakim Abdi
Department of Physical Geography and Ecosystem Science
Lund University, Sweden

Supervisor: Jonas Ardö
Department of Physical Geography and Ecosystem Science
Lund University, Sweden

Exam committee:

Petter Pilesjö
Department of Physical Geography and Ecosystem Science
Lund University, Sweden

Niklas Boke Olén
Department of Physical Geography and Ecosystem Science
Lund University, Sweden

Acknowledgments

I would like to thank and acknowledge:

The Swedish Institute for awarding me the study program scholarship

My supervisors Hakim and Jonas for their guidance

My friends in Lund for their support all the time

My family for giving me the strength

My mother for all the love

Abstract

Tree vegetation is an essential element in the daily life of the people in the Sahel region of Africa. It is also considered as a robust indicator of the Sahel ecosystem status and health. In this thesis, a method to estimate tree vegetation was developed and used in mapping the tree canopy cover in semi-arid Sahel. The developed method utilized Normalized Difference Vegetation Index (NDVI) as the predictor variable coupled with estimations of tree canopy cover from Google Earth imagery as the response variable. The developed estimation regression was applied in the Sahel of Africa for the dry season (November to May). The results showed a strong correlation between NDVI derived from Landsat 8 imagery and Tree Canopy Cover (TCC) estimations from Google Earth imagery. The developed method errors were evaluated using two different validation approaches. Moreover, two estimation regressions were developed using NDVI products from Moderate Resolution Imaging Spectroradiometer (MODIS) and Global Inventory Modeling and Mapping Studies (GIMMS). The correlation between MODIS and GIMMS NDVI was weak which could be due to the coarse spatial resolution of these NDVI products. Mapping tree cover in the Sahel using Landsat 8 derived NDVI require high computational power and large storage capacity. Therefore, Landsat 8 NDVI based estimation regression was applied to MODIS and GIMMS NDVI products to the map tree canopy cover for the entire Sahel. All the datasets used in this study is available for public use, and therefore this method is applicable for more development and improvements.

Keywords: Tree cover, Sahel, NDVI, Google Earth, Landsat 8

Table of contents

List of Figures:

List of Abbreviations:

NDVI	Normalized Difference Vegetation Index
MODIS	Moderate Resolution Imaging Spectroradiometer
OLI	Operational Land Imager
GIMMS	Global Inventory Modeling and Mapping Studies
TCC	Tree Canopy Cover
FAPAR	Fraction of Absorbed Photosynthetically Active Radiation
AGB	Above Ground Biomass
RMSE	Root Mean Squared Error
OLS	Ordinary Least Squares

Chapter 1: Introduction

1.1 Background and Motivation

Trees are essential to the lives of the people in the Sahel region of Africa, particularly through agroforestry, timber extraction, and the provision of non-wood products such as food, fodder, and medicine (Gonzalez et al. 2012; Karlson et al. 2015;). Forests and woodland support livestock during the long dry season by providing woody fodder, which is high in water content (Abrol 2013). Fuelwood, including charcoal, is the primary source of household energy in the region. In West Africa, it is estimated that fuelwood makes up 85 percent of total household energy consumption (Abrol 2013).

The Sahel is a transition zone between the dry Sahara Desert in the north and humid Guinean zone in the south. The Sahel is known to be highly sensitive to environmental changes such as the prolonged droughts in the 1970s and anthropogenic factors such as the increase of the human population and the sharp increase in the stock numbers (Vincke, Diedhiou, & Grouzis, 2010). Eklundh & Olsson (2003) observed a positive trend in vegetation greenness in Sahel from 1982 to 2000, which was attributed to the herbaceous and shrub layer (Herrmann & Tappan 2013). Studies focusing on woody vegetation may contribute to understanding the greening Sahel phenomena. Woody vegetation is an essential component of the Sahel ecosystem and a more robust indicator of ecosystem status and health than herbaceous biomass (Herrmann & Tappan, 2013), which varies between seasons. The vast areal extent of Sahel makes it an important component of the global climate system by sequestering and storing substantial amounts of carbon in woody biomass (Karlson et al. 2015). At present, the tree canopy cover is subject to increasing pressure from intensified land use and climate change (Karlson et al. 2015). Hiernaux et al. (2009) described massive mortality of woody plant populations throughout the Sahel which is consequently linked to high risks of species diversity losses. The decrease in the woody cover in the Sahel may contribute to wind erosion, reduced organic soil. Recent studies, such as Brandt et al. (2015), highlighted the controversy in the analysis of Sahel greening or degradation status based on the sources of earth observation data. The study discussed scale issue since the coarse-

scaled vegetation trend analysis revealing greening Sahel and other local-scaled studies showing degradation and greening at the same time. A study by Sendzimir et al. (2011) reported a dramatic reforestation of a massive scale (more than 5 million hectares) in Niger, which was attributed to interactions across biophysical, economic, and social domains. A recent study by Karlson & Ostwald (2016) investigated the hands-on application of earth observation data in the Sudano-Sahel zone from 1977 to 2014. They showed that studies on tree canopy cover, i.e. the proportion of land area covered by tree crowns as viewed from above, are scarce in comparison with other vegetation mapping methods. Despite the importance of the tree canopy cover as an environmental indicator of the health of ecosystems, only 24 out of the 268 peer-reviewed articles in the Karlson & Ostwald (2016) study relate to tree canopy cover as their main research topic. Thus, it is important to devise a rapid and cost-effective method to map tree canopy cover in Sahel. Such an approach could help the local authorities and the global partners to develop an understanding of the complex mechanisms underlying the greening of the Sahel.

1.2 Research Question

This study aims at estimating tree canopy cover for the Sahel using satellite remote sensing data and a Google Earth-derived training and validation dataset. A linear regression model will be developed to map the tree canopy cover of the region. The developed model will be based on the relationship between dry season tree canopy cover and Normalized Difference Vegetation Index (NDVI) derived from the following Earth observation datasets (1) Moderate Resolution Imaging Spectroradiometer (MODIS), (2) Landsat 8 Operational Land Imager (OLI), and (3) Global Inventory Modeling and Mapping Studies (GIMMS3g). These three datasets were selected based on their different spatial resolutions, ranging from 30 meters (Landsat 8) to 8 km (GIMMS3g), to study the effect of scale on the modeling process. Thus, the research questions are:

1. Can tree canopy cover for the entire Sahel be modeled using Google Earth derived training and validation data?

2. What is the effect of scale (i.e. spatial resolution) on the tree canopy cover that results from Landsat, MODIS, and GIMMS3g Earth observation data?

1.3 Study Area

The Sahel is an eco-climatic region extending from the Atlantic Ocean in the west to the Red Sea in the east (Figure 1). The Sahel represents the transition from the dry Sahara Desert in the north to the humid Guinean zone in the south and includes 11 sub-Saharan countries (Figure 1). Low and varying rainfall marks the region, amounting to 100–600 mm per year on average in the Sahelian zone and between 600 and 1500 in the Sudanian zone (Jamali et al. 2014). The rainy season is linked to the West African Monson with a length of 1-4 months, and an annual peak in precipitation in August (Brandt et al. 2016). The mean annual rainfall and soil characteristics control the structure and the floristic composition of the vegetation in the zone. The vegetation in the Sahel is composed of annual grasses and a sparse tree cover, where the proportion of trees and shrubs, the height of vegetation and the vegetation density increase towards the south (Karlson, 2015).

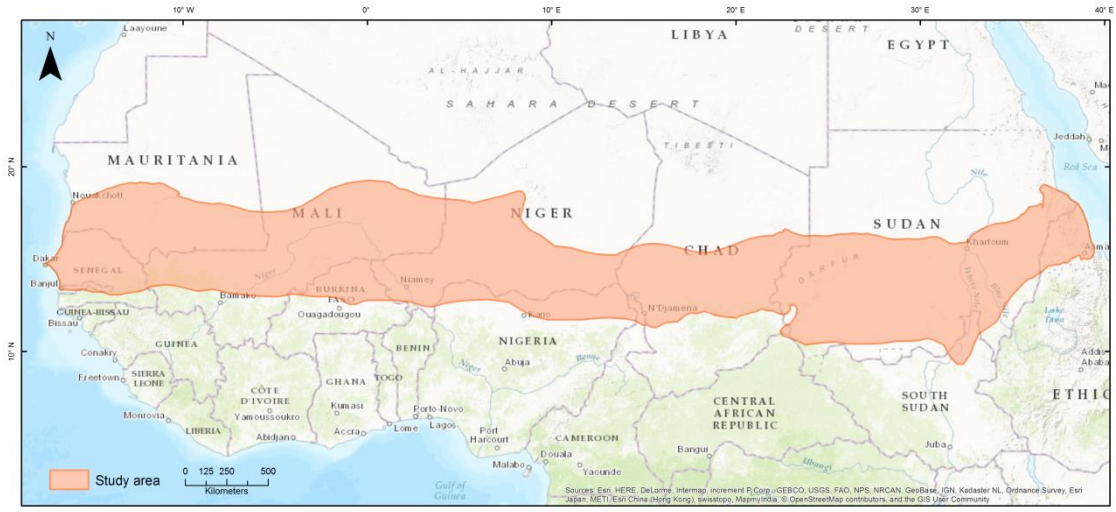

Figure 1: The semi-arid Sahel is categorized by the annual rainfall ranges from 100 mm in the northern boundary to 600 mm in the south (Nicholson 2013). The background base map was acquired from Esri ArcMap 10.

The population density varies across the region and has increased faster than in the rest of the world in the past decades according to statistics from the United Nation (UNEP 2011). From 1960 to 1995, the population increased from 21 million people to 46 million in the nine countries of Central and West Africa (Gonzalez et al. 2012). While between 2000 and 2010, the population of the entire Sahel grew from 367 million to 471 million at an average rate of 2.8% per year and is projected to increase to nearly one billion by 2050 (Abdi et al. 2014). Approximately 80% of the population relies on subsistence agriculture and livestock herding, much of which is practiced in traditional agroforestry systems (e.g. managed woodlands) (Boffa 1999). Trees in the Sahelian are fundamental to the livestock production system and social practices as they provide charcoal, fuel wood, and medicine among other things. Tree decline affects the production and quality of the herbaceous layer and the welfare of livestock and pastoralists alike (Vincke et al. 2010). Degradation of woody resources may have significant social and ecological consequences such as population migration and soil degradation (Sop & Oldeland 2011).

1.4 Thesis Outline

Chapter 1 presents the introduction and the relevance of the study, the study area, and thesis questions.

Chapter 2 presents a review of recent literature about tree canopy cover mapping and remote sensing application with a focus in the Sahel and other similar ecosystems.

Chapter 3 describes the multi-source, multi-scale data and the methodology which was used to estimate the tree canopy cover.

Chapter 4 illustrates the results of the correlation between vegetation indices (Landsat, MODIS, and GIMMS3g) and estimations from Google Earth imagery.

Chapter 5 discusses the output of the study and study limitations.

Chapter 6 contains the conclusions and future research suggestions.

Chapter 2: Literature Review

2.1 Introduction

This chapter represents a review of the literature on woody vegetation in the Sahel, the use of remote sensing data and methods for woody plant estimation and mapping. Droughts events in the 1970s and 1980s, desertification, land degradation, poverty, food security and climate change have made the Sahel a hot spot for research over the last four decades (Mbow et al. 2014).

2.2 Woody Vegetation in the Sahel

Estimating the woody canopy cover in Africa savannas, particularly in the Sahel using remote sensing data and methods has been a research area for several years (Sankaran et al. 2005.; Hiernaux et al. 2009; Wu et al. 2013). Tree canopy cover properties, such as density and species richness can reveal long-term trends in the Sahelian vegetation which is undetectable through monitoring herbaceous vegetation (Gonzalez et al. 2012).

Many studies that are focused on tree cover mapping or change detection use in-situ measurements for specific sites (Herrmann & Tappan 2013 and Gonzalez et al. 2012), and in some cases, combine in-situ measurements with local interviews. Other studies combined in-situ measurements with remote sensing derived indices such as NDVI from MODIS or Landsat. Wezel (2005) conducted interviews with rural people in five case studies from three West African Sahel countries (Burkina Faso, Senegal, and Niger) to quantify the change in woody vegetation based on their local knowledge. Hiernaux et al. (2009) investigated the dynamics of woody plants in response to climate change in Sahel with a case study from Gourma, Mali from 1984 to 2006 using data on rainfall, soil and woody plant species from different sources. Their results show an

increase in the population density and canopy cover in the study area and suggest a reconsideration of the sampling and observation methods previously used in the survey area. Vincke et al. (2010) studied the dynamics and structure of woody vegetation in Ferlo (Senegal) for the period between 1976 and 1995 based on in-situ measurements of a 0.25 square kilometer experimental area. They found that the woody cover was in degradation in both study sites.

Interviewing different ethnic communities in Burkina Faso, Sop & Oldeland (2011) explored the decline in woody species in the Sahel by contrasting the alleged (re)greening in the region and suggesting further degradation of woody resources. They emphasized the role of local ecological knowledge for assessing vegetation dynamics and environmental change over time. Herrmann & Tappan (2013) conducted a study in a region in central Senegal to examine changes in woody vegetation abundance and composition in selected sites using a botanical inventory of woody vegetation species, repeat photography, and perceptions of local land users. Their results show increases in woody vegetation occurred only in the shrub layer and a loss in species richness.

The field measurement and the meeting with the local population can provide information about the woody cover older than the records of the historical remote sensing data. In-situ measurements are quite challenging and expensive. Their results will be limited to the study area due to the spatial heterogeneity of the Sahel (Mbow et al. 2014). Remote sensing data and methods can provide an auxiliary or an alternative to the method mentioned above for estimating and mapping woody canopy cover in Sahel.

2.3 Remote Sensing of Woody Canopy Cover

Remote sensing data, acquired by optical and microwave sensors mounted on satellites, aircrafts, and unmanned aerial vehicles are important alternative sources of information for mapping and monitoring the woody vegetation. The advantages include low costs in comparison to in-situ measurements, the high frequency of the data acquisition, and availability of global coverage of remote sensing data via web portals, low cost or cost free data, and a wide range of resolutions from both a spectral and spatial perspective. The availability of historical records of remote sensing data in the form of aerial photos

and the rich archive of vegetation indices derived from NASA Earth observation satellites are additional assets for woody cover modeling and mapping.

Optical remote sensing is commonly used in the mapping and monitoring of woody vegetation, while active remote sensing is rarely used. Mitchard et al. (2009) found that PALSAR HV backscatter responds strongly to Above Ground Biomass (AGB) in a consistent manner across four African sites, one of them representing a transition zone between savanna and forests in Cameroon, which consists of a similar vegetation structure as the Sahel. The study suggested that above ground woody biomass can be predicted using radar data for large areas dominated by differing vegetation types with useful accuracy.

The remote sensing of the change in tree cover attributes (e.g. canopy cover and tree density) have primarily been analyzed using high or medium resolution imagery to separate trees and shrubs from the herbaceous vegetation that dominates the satellite signal during the growing season. However, recent research has shown that coarse resolution NDVI data acquired during the dry season is an interesting alternative for analyzing tree cover changes over larger spatial extents (Karlson & Ostwald 2016). Rasmussen et al. (2011) combined high spatial resolution QuickBird imagery with a field survey in Senegal for a 10 km x 10 km study area and developed allometric models for three main tree species in the area. The developed model in the study demonstrates the potential of using high-resolution QuickBird imagery for tree inventory analysis. Gonzalez et al. (2012) used field measurements, aerial photos, and IKONOS imagery to detect the decline in the tree species in five countries in the West African Sahel. The result showed declination in trees density and trees species richness from 1960 to 2000. Furthermore, the study linked the decline trees density and species richness to increasing temperature and decreasing precipitation. Developing a linear model to estimate the woody biomass from NDVI Using the Republic of Sudan as a study area, Wu et al. (2013b) mapped woody biomass by deriving NDVI from Landsat and MODIS data. The developed model offered a capable method for year-round woody biomass estimation. The obtained results were compatible with results from other authors and the available ground-truth data. Many studies from the mentioned above utilized high spatial resolution satellite imagery as an alternative or auxiliary to the inventory filed measurements.

High-resolution aerial photos or space-borne imagery are widely used to recognize trees as objects for mapping and change detection studies. These data are often in commercial domain, which restricts their use in both research and operational monitoring. Brandt et al. (2014) investigated the relationship between the canopy cover and soil properties in Senegal. Soil map was derived from field survey, while canopy coverage was modeled using high-resolution RapidEye imagery and NDVI derived from Landsat data. Interviews with the local population supported by existing literature were used as the basis for investigating the environmental changes, climatic and erosion vulnerability for each soil type. The study highlighted the importance of soil properties in the context of ecosystem resilience and ecological change. Karlson et al. (2015) evaluated the use of Landsat 8 Operational Land Imager (OLI) NDVI for mapping tree canopy cover (TCC) and AGB while using field measurements and Worldview2 imagery as a reference dataset. The results showed a strong correlation between NDVI and TCC than NDVI and AGB. The study suggested higher spatial resolution data (e.g. the upcoming Sentinel-2) will be suitable for mapping tree cover attributes in Sahel. A study by Brandt et al. (2016) explored the relationship between satellite-derived a seasonal metric of Fraction of Absorbed Photosynthetically Active Radiation (FAPAR) and in situ measured woody cover to map the woody cover in Sahel for the 1999 - 2013 period. The study compared the estimated woody cover map with the global tree cover product MOD44B and found that the expected woody cover to be nine times higher than the global tree cover.

Studies about tree cover properties usually focus in examining tree cover density, species richness, and AGB. Each one of these properties can reveal information about the ecosystem status. Herrmann and Tappan (2013) detected an increase in woody vegetation density, but mainly in the shrub layer, while the number of trees decreased. In general, they found a loss in species richness and a shift towards more xeric species. The loss in species richness is interpreted as an indicator of degradation in some studies(Res & Gonzalez 2001), while Herrmann and Tappan (2013) pointed out that it could also be seen as an adaptation of the ecosystem to more arid climate conditions during the dry years until the mid-1990s.

Developing empirical relationships between in-situ measurements and remote sensing derived vegetation (e.g. NDVI) indices is used in some studies (Wu et al. 2013a; Brandt et al. 2014; Brandt et al. 2016) for mapping the tree cover. There is some reticence to the use of NDVI as a proxy to assess Sahel woody vegetation cover trend, mainly that NDVI tracks the herbaceous vegetation which varies according to the rainfall levels across the season while the second restraint is the time limitation of the NDVI records. The annual NDVI record started in 1982, while the region witnessed a major climatic event earlier such as the 1970s drought (Gonzalez et al. 2012). However, other studies (Wu et al. 2013a; Brandt et al. 2016) suggested acquiring NDVI data in the dry season, due to the absence of the herbaceous vegetation.

The geographical distribution of the woody vegetation research is uneven in the Sahel, with dominance within a few countries in West African Sahel (e.g., Mali, Burkina Faso, Niger, and Senegal). This pattern is driven by multilateral research collaborations, availability of in-situ data and research infrastructure, and political stability (Karlson & Ostwald 2016). Local scale research has shown that climate change and land use change have caused degradation of the tree cover in different part of the Sahel (Res & Gonzalez 2001; Gonzalez et al. 2012). The detection and attribution of tree cover change can guide future measures for improving natural resource management in the Sahel. Tree cover monitoring by remote sensing on larger spatial scales is therefore needed to provide comprehensive descriptions of the process and establish whether it is operative at regional or continental scales (Karlson & Ostwald 2016). Improving capacity and availability of remote sensing tools and data may encourage more research that can aid in developing sustainable policies in response to the change in the vegetation dynamics in Sahel.

Chapter 3: Data and Methods

3.1 Introduction

In this chapter, the data and methods will be presented. The first two sections (3.2 and 3.3) describe the different data sources, associated metadata, pre-processing procedures, and data management. Section 3.4 describes the methodology, including the development and validation of the regression to map tree canopy cover using Google Earth imagery and satellite Normalized Differences Vegetation Index (NDVI) from different.

3.2 Reference Dataset

Google Earth imagery was used to assemble the reference dataset for Tree Canopy Cover (TCC), which is the fraction of land area covered by tree crowns when viewed from above. TCC is estimated from images collected during the dry season (November to May) for the period of 2010-2015. TCC is a widely-used variable in land cover definitions, for example, areas with 10–30% TCC are often classified as woodlands (Karlson et al. 2014).

Google Earth, released in 2005, provides global coverage of high-resolution satellite imagery. There is two main providers the source satellite imagery to Google Earth, DigitalGlobe, and Astrium. Both companies get their imagery from different satellite constellations. DigitalGlobe satellites include IKONOS, QuickBird, WorldView-1, WorldView-2, GeoEye-1, and WorldView-3. Appendix Table 1 shows the specification of the products from DigitalGlobe. Astrium imagery is acquired from Pléiades 1A and 1B satellites with a ground sampling distance of 0.5 m in the panchromatic band and 1.5 m in multispectral bands. SPOT-6 and SPOT-7 are also part of Astrium satellites constellations. The spatial resolution for both satellites is 1.5 m in the panchromatic band and 6 m in the multispectral bands (Appendix Table 2). Google Earth offers a rich archive of historical imagery which can be accessed using the historical imagery tool.

To sample TCC in the Sahel, 500 reference sample points were collected across the study area (Figure 2). Because of the region's semi-arid geography, the points were not randomly sampled since that would lead to a disproportionally large percent in open areas. Instead, selection of the points was made to ensure a normal distribution of tree canopy cover ranging from 0 – 100% (Figure 3). After locating the points, Esri ArcMap 10 was used to draw one hectare (100 x 100 m) plots around them. The plot size was chosen because (1) it is a standard unit of field measurement in previous studies (Vincke et al. 2010; Spiekermann et al. 2014; Oduori et al. 2011), and (2) it is broad enough to encompass several tree crowns but is not too large to be labor intensive. Additionally, the size of the plot is a compromise between the 30-m cell size of Landsat 8 and the 250-m cell size of MODIS. The reference TCC dataset and NDVI derived from Landsat 8 will be used to develop a TCC-NDVI linear regression model. All of the 500 reference polygons were saved in ArcMap shapefile format with a unique name for each plot. The polygons were later exported to Keyhole Markup Language (KML) files. The KML data were displayed in Google Earth and screen shots of the plots were collected using the Snipping Tool from Microsoft. The screenshots were saved in Portable Network Graphics (PNG) format with a unique name for each plot which included a matching name for the same plot in the ArcMap shapefile.

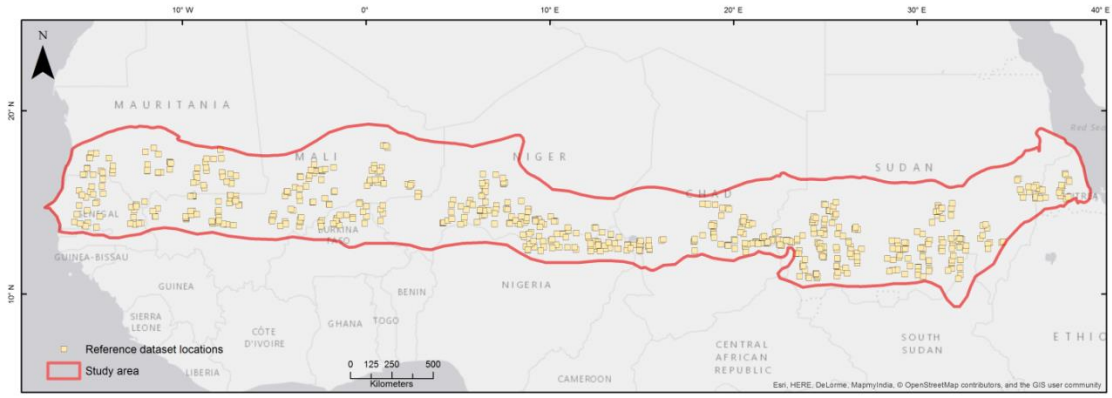

Figure 2: Locations of the reference data collected using Google Earth imagery. Note: The size of the reference dataset icons in the map was exaggerated show the distribution over whole Sahel. The background base map was acquired from Esri ArcMap 10.

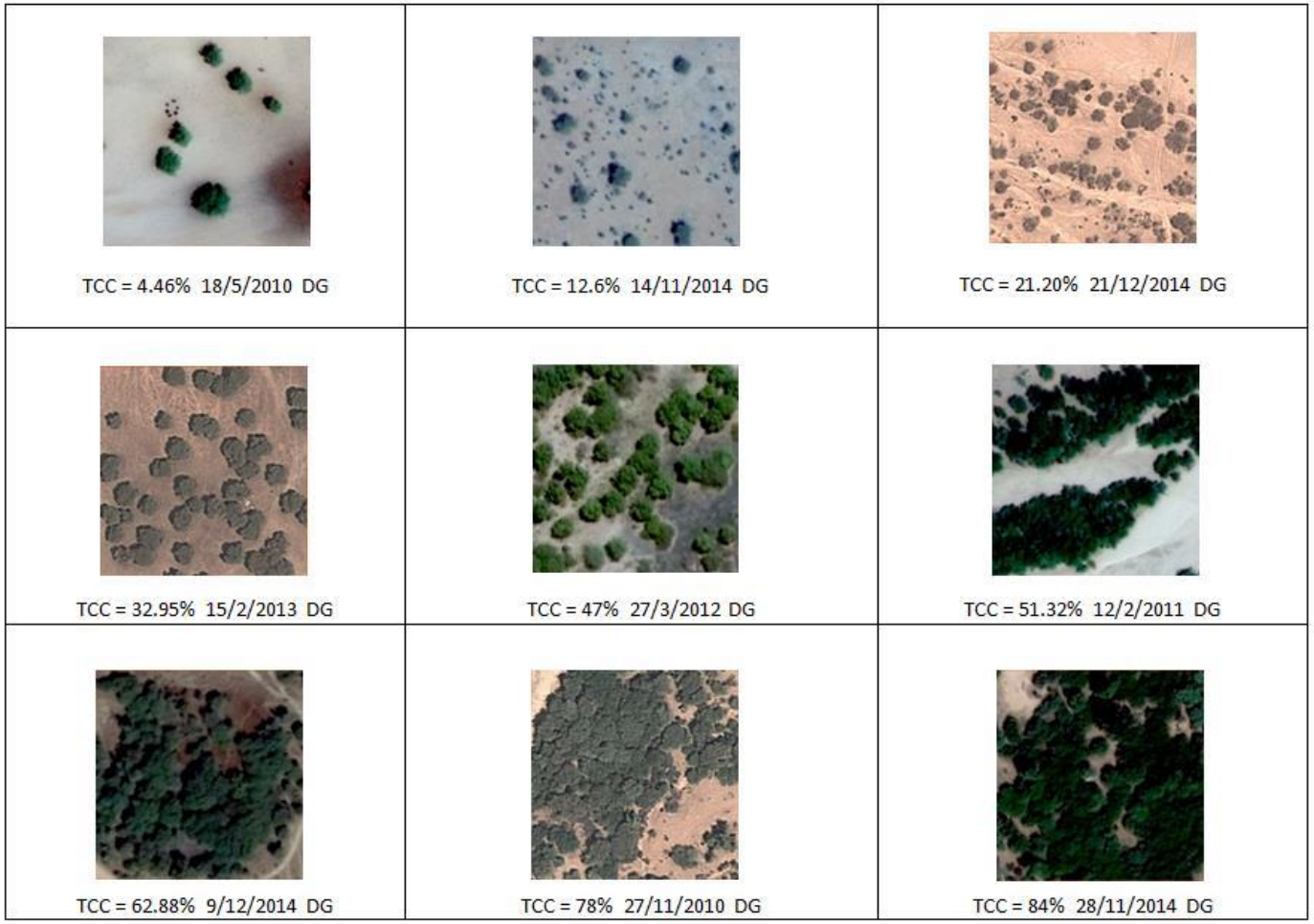

Figure 3: Nine examples of the reference dataset showing TCC percentage, acquisition date, and satellite imagery provider. TCC varies between 4.46% in the top left sample to 84% in the lower right sample. DG stands for DigitalGlobe the imagery provider.

The percentage of TCC in each plot was estimated using an image processing software (Paint.Net, http://www.getpaint.net/) that provides the capability of selecting pixels in a picture with the same color(s) or shades. Estimation procedure included exporting screenshots of each plot from Google Earth and saving it as images in PNG format. Afterward, each image was opened in Paint.Net software. Each plot image was classified into two classes - Tree or No Tree Using a selection tool. The former included pixels with greenish coloration and the latter with pixels with brighter colors representing the background soil. The number of pixels in each class used to quantitatively estimating the percentage of TCC in each plot and later saved in Microsoft Excel. Figure 4 demonstrates screenshots of the Paint.Net software.

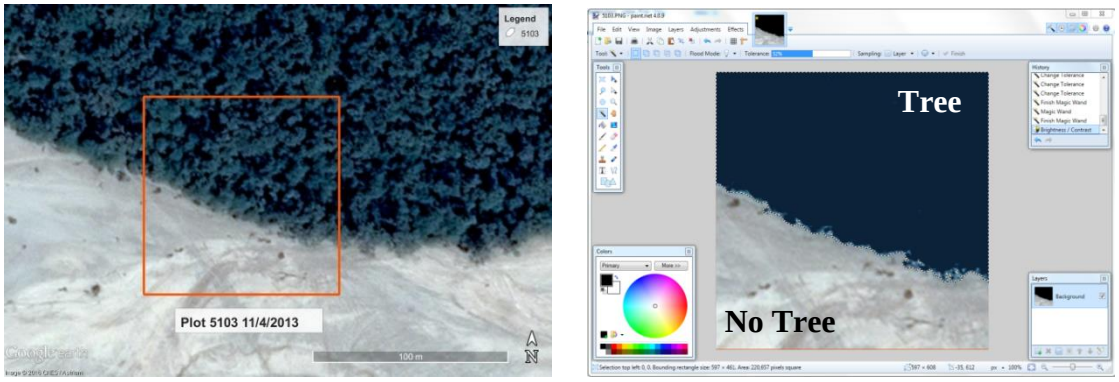

Figure 4: Estimation of TCC through Paint.Net software. To the left is screenshot from Google Earth, the orange-colored rectangle is the reference data plot, which was then transferred to Paint.Net on the right. Pixels are classified into two categories – those that have TCC and those that represent bare soil.

The main limitation of this method is that it can be applied only in the plots where there is an apparent difference in reflectance between trees and background soil. However, the reflectance can be treated by enhancing the contrast to differentiate trees from the background soil. Problems can also arise with shadows generated by trees. The shadow limitation can be overcome by using satellite images recorded at noon at nadir geometry or, more generally, in situations where the sun is immediately behind the sensor (Rasmussen et al. 2011) which was assured during the sampling process.

3.3 Satellite-derived NDVI

3.3.1 NDVI

Vegetation indices are used for vegetation monitoring widely in the large-area (Lillesand et al. 1989). They are useful measures of the physiologically functioning surface greenness of a region (Tucker 1979). This study utilized Normalized Differences Vegetation Index (NDVI) as the predictor variable in the estimation of TCC. NDVI is a commonly used vegetation index and is described by Equation 1:

$$NDVI = \frac{NIR - RED}{NIR + RED} \qquad (1)$$

Where, *NIR* is the spectral reflectance in the near infrared wavelength (0.85–0.88 μm) and *RED* is the spectral reflectance in the red wavelength (0.64 -0.67 μm). Availability of long-term (30+ years) NDVI archive makes it useful in vegetation phenology studies (Jin & Eklundh 2014). In this study, three different NDVI products were used. Landsat 8 NDVI was used to develop a TCC-NDVI linear regression model. The Landsat 8 NDVI was averaged and up-scaled to two different spatial resolutions (250m to match MODIS NDVI and 8 km to match GIMMS3g NDVI). Two new linear regression models were developed and compared to the earlier regression model.

3.3.2 Landsat 8 NDVI

Landsat 8 was launched in February 2013 and continues the 40 years of the Landsat Earth observation archive. The Operational Land Imager (OLI) onboard Landsat 8 has several improvements over its predecessors – the Thematic Mapper (TM, Landsat 4 and 5) and the Enhanced Thematic Mapper (ETM+, Landsat 7). Such a enhancements provide significant improvements in the ability to detect changes on the Earth's surface (Irons et al. 2012) one of which is tree canopy cover. Thus, Landsat 8 represents an interesting data source for remote sensing based tree cover mapping.

Landsat data is available on the Earth Explorer platform of the United States Geological Survey (USGS, http://earthexplorer.usgs.gov/). 50 Landsat 8 scenes were acquired to cover the study area. The scenes were chosen to be from the dry season (November to

May) which acquisition dates and scenes are shown in Appendix 1. The scenes were distributed across the Sahel to match with the reference dataset (Figure 5). Two spectral bands were used calculate the NDVI. A pre-processing operation to calculate NDVI was performed by converting the digital number of the red and NIR bands to top-of-atmosphere reflectance (Lillesand et al. 1989). Dark Object Subtraction atmospheric correction was also performed, based on the equation from Chavez (1988). The corrections were carried out using the Semi-Automatic Classification Plugin (Congedo 2014)in QGIS 2.2 Valmiera.

NDVI was calculated for the 50 scenes by using Equation 1. The images were cloud free due to the data set being collected during the dry season. NDVI values below 0.1 were masked out as they may not represent vegetated areas (Jeong et al. 2011).

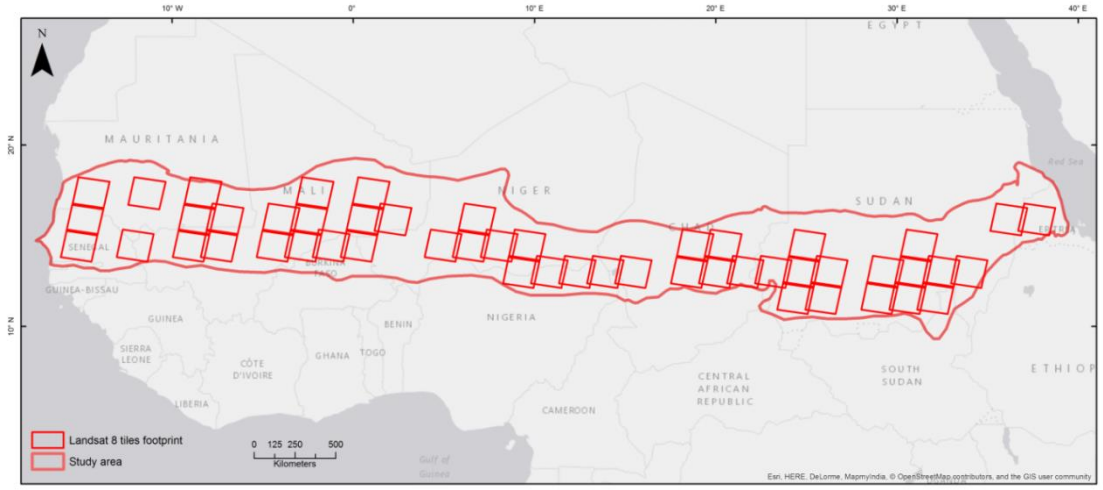

Figure 5: Landsat 8 tiles footprint. 50 scenes were downloaded, pre-processed, and used to calculate NDVI. The background base map was acquired from Esri ArcMap 10.

3.3.3 MODIS NDVI

Moderate-resolution imaging spectroradiometer (MODIS) NDVI products are atmospherically corrected by using bi-directional surface reflectance and have been masked for water, clouds, heavy aerosols, and cloud shadows (Jamali et al. 2014a). In this study, the L3 Global MODIS Terra NDVI 16-Day composite images with a 250-m spatial resolution (MOD13Q1 V005 product) from November 2014 were used. Six tiles were collected to cover the study area and were downloaded from the Land Process Disturbed Active Archive Centre (LP DAAC) website

(https://lpdaac.usgs.gov/data_access/data_pool). MOD13Q1 products provide information about the quality of the NDVI on pixel level. The information that was used to examine MOD13Q1 pixel quality is based on a reliability classification. This classification scheme contains ranked values describing overall pixel quality. Table 1 illustrates the different levels of quality and their descriptions.

Table 1: MOD13Q1 pixel reliability
(https://lpdaac.usgs.gov/dataset_discovery/modis/modis_products_table/mod13q1)

Rank key	Summary QA	Description
-1	Fill/No Data	Not Processed
0	Good Data	Use with confidence
1	Marginal data	Useful, but look at other QA information
2	Snow/Ice	Target covered with snow/ice
3	Cloudy	Target not visible, covered with cloud

After evaluating the dataset, 96% of the pixels were classified as “good data” and therefore can be used with confidence. Only 4% of the pixels were classified as “marginal data” which suggests that they can be utilized, but more information should be extracted from the vegetation quality layer. Figure 6 illustrates MOD13Q1 NDVI for the Sahel.

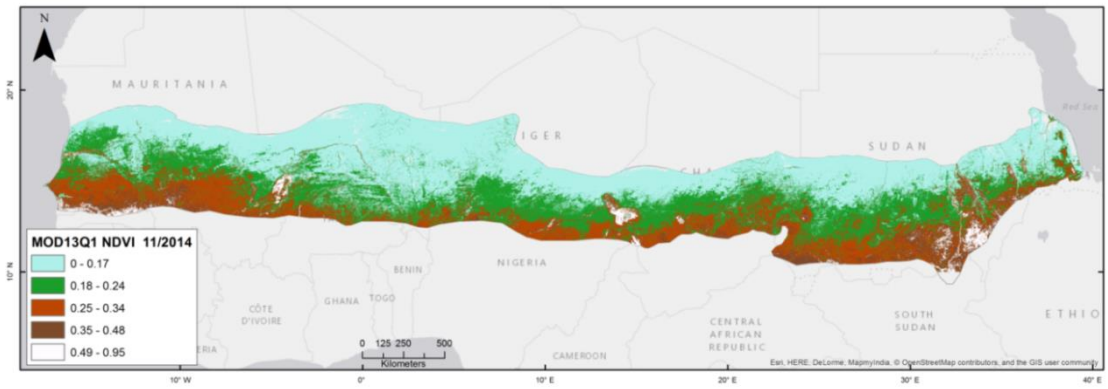

Figure 6: MOD13Q1 NDVI mosaic for November 2014. The background base map was acquired from Esri ArcMap 10.

3.3.4 GIMMS3g NDVI

The third source of NDVI for this study is GIMMS3g (Figure 7); it is a product of Global Inventory Monitoring and Modelling System (GIMMS) project. This dataset is available in biweekly NDVI images. It has been combined into a monthly image using a maximum value composite function to minimize the influence of clouds (Fensholt & Proud 2012). It covers the period from July 1981 to December 2013. It is referred to as NDVI3g (third generation GIMMS NDVI from AVHRR sensors). The AVHRR sensors used to construct the dataset were flown on several NOAA (National Oceanic and Atmospheric Administration) satellites. The NDVI3g has been corrected for factors that do not relate to changes in vegetation greenness and an improved cloud masking as compared to older versions of the GIMMS dataset (Vrieling et al. 2013). NDVI3g comes in 8-kilometer spatial resolution. For comparative reasons, only data from December 2013 was used.

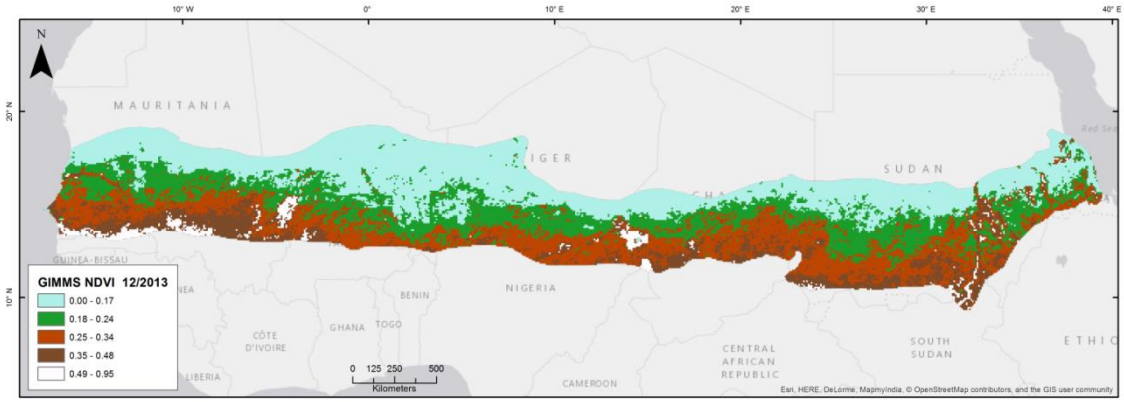

Figure 7: GIMMS3g NDVI for December 2013. The background base map was acquired from Esri ArcMap 10.

3.4 Methodology

To fulfil the objective of this study which was mapping tree canopy cover in semi-arid Sahel, a TCC-NDVI linear regression model was developed and validated, by coupling TCC estimated from Google Earth imagery with remote sensing NDVI derived from Landsat 8 imagery. The developed regression was compared with medium and coarse spatial resolution NDVI products (MOD13Q1 and GIMMS3g). The regression was

applied to MODIS NDVI to obtain full coverage of Sahel. Figure 8 illustrates the methodology and the materials.

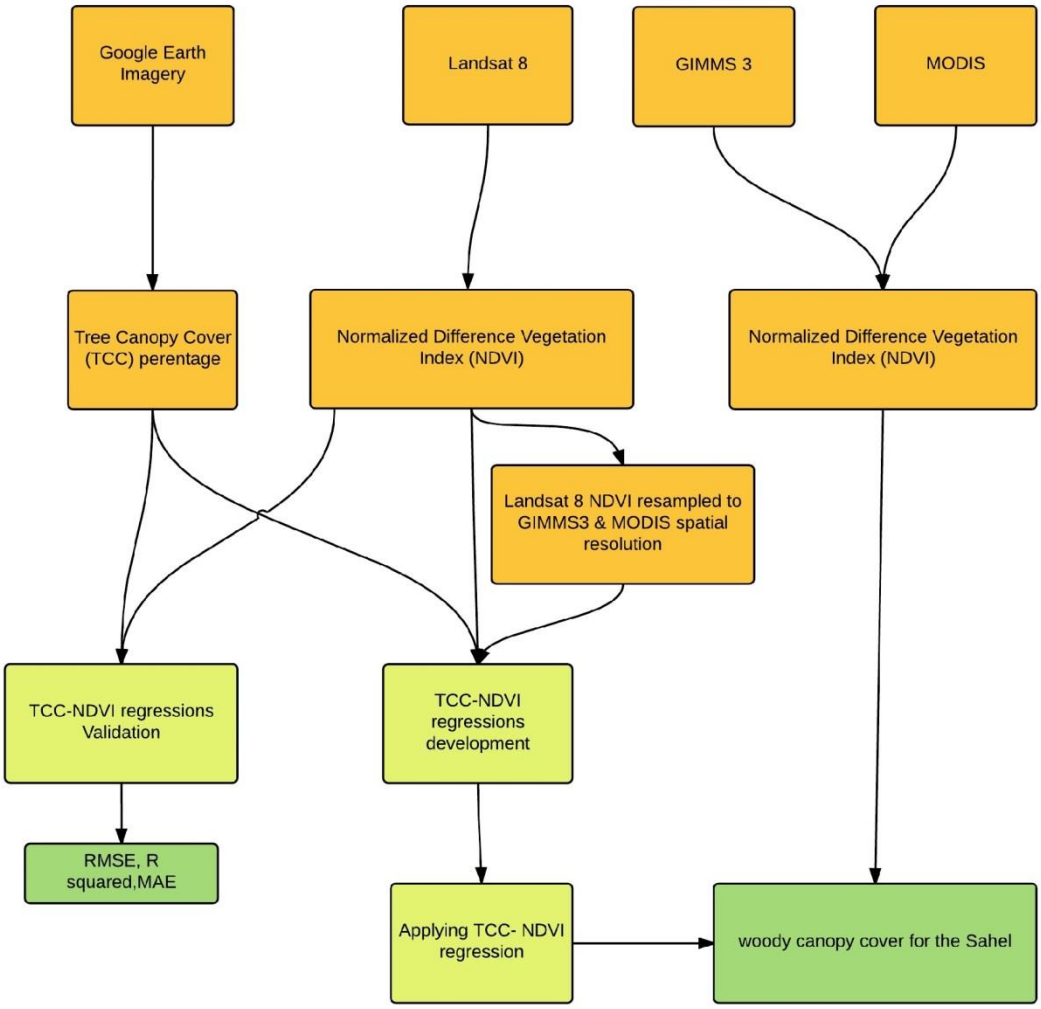

Figure 8: Flowchart of the methodology.

3.4.1 TCC-NDVI model development

Seventy percent of the reference dataset was used as a training set to develop the TCC-NDVI linear regression model. The remaining 30% was used for validation. Some of the reference dataset plots showed burned trees which could introduce errors in the estimation. In other plots, there was green herbaceous vegetation even in the dry season. The reason behind the existing of the herbaceous vegetation could be that areas that are located near to permanent water sources like rivers or lakes are not dependent on rainfall. A total of 76 plots were removed from the analysis to reduce the effect of the

herbaceous vegetation and burned trees. The total number of the plots after the removal of problematic ones was 424. The Zonal Statistics tool in ArcMap was used to extract the corresponding NDVI values to each reference data set plots. As the Landsat 8, NDVI spatial resolution is 30 m while the reference dataset plot size is 100 x 100 m, a mean NDVI value was extracted for the Landsat pixels which were completely within the reference plot. Ordinary least squares (Steel et al. 1980) linear regression model was constructed using TCC of the 297 reference plots (70%) and Landsat 8 derived NDVI. OLS regression has been the most common choice for fitting the equation between the dependent and independent variables (Karlson et al. 2015). In this study, TCC estimated from Google Earth imagery reference data is the dependent variable. And satellite-derived NDVI is the independent's variables. The regression will provide a prediction of tree canopy cover over the extent of the satellite NDVI imagery

3.4.2 TCC-NDVI model validation

The reference data set has been split into training data set (70% of the reference sample points) and test data set (30% of the reference sample points). Then using the developed linear regression model the TCC of the test dataset were calculated. In addition to the coefficient of determination (R^2) that results from the regression analysis, the root mean squared error (RMSE) and mean absolute error (MAE) were computed using equations (2 and 3):

$$RMSE = \sqrt{\frac{\sum_{i=1}^{n}(X_{est,i} - X_{cal,i})^2}{n}} \quad \textbf{(2)}$$

$$MAE = \sqrt{\frac{\sum_{i=1}^{n}(X_{est,i} - X_{cal,i})}{n}} \quad \textbf{(3)}$$

Where X_{est} is estimated from Google Earth TCC% values and X_{cal} is calculated using the regression values.

3.4.3 Applying TCC-NDVI regression

The developed TCC-NDVI regressions were based on Landsat 8 NDVI. Also, more two other linear regressions model were developed based on Landsat 8 NDVI resampled to the spatial resolutions of GIMMS3 and MOD13Q to facilitate intercomparison with those products. Due to the Sahel being a vast region many Landsat 8 scenes would be needed (165 scenes). This is challenging considering data amount and the required processing capacity. Therefore, it would be beneficial to apply the Landsat-based TCC regression model (the one developed using resampled Landsat 8 NDVI) on products that cover larger areas with lower spatial resolution and accordingly taking up less storage space and requiring less processing power. MOD13Q1 and GIMMS3g NDVI products were used to estimate TCC based on the developed regression models.

Chapter 4: Results

4.1 Introduction

This chapter presents the results of the study in four sections. The first section discusses the model development and statistical significance of the linear regression. The second section presents the results related to regression validation, and the third section focuses on the outcome of the application of the regression for the GIMMS and MODIS datasets. The last section is a comparison between the NDVI from the three different sources.

4.2 Model Development

4.2.1 Linear regression using Landsat NDVI

As stated in the previous chapter, 70% of the reference dataset was used to develop the TCC-NDVI regression. Equation 4 describes the developed regression using OLS regression.

$$y = 155.48x - 18.512 \quad (4)$$

Where, y is the estimated tree canopy cover (TCC, %) and x is Landsat 8 NDVI.

There was a robust and significant correlation ($R^2 = 0.81$, $P < 0.005$) between dry season Landsat 8 NDVI and TCC estimations from Google Earth imagery (Figure 9). Using OLS, 81% of the variance was explained ($R^2 = 0.81$). The developed model (Equation 4) was used to predict TCC in the Sahelian dry season (November to May). TCC percentage among the estimated training dataset varies from 0% to 99.9% with a mean of 47.73% while Landsat 8 NDVI ranges from 0.13 and 0.78 with an average of 0.42. Applying the developed regression can lead to overestimating in TCC values (TCC >100%) which could be a result of the saturation of NDVI observation at higher leaf area indices(Jamali et al. 2014b).

Residual analysis was performed to ensure the robustness of the regression; the output is shown in Figure 10. According to the residual analysis, no findings were found that significantly violated the assumptions of linear regression. The relationship followed a linear trend in general while the distribution of the residual was normal. Additionally, there was a relatively similar spread of the residuals along the range of the predictor variable. Finally, no influential outliers were detected by the residual-leverage analysis.

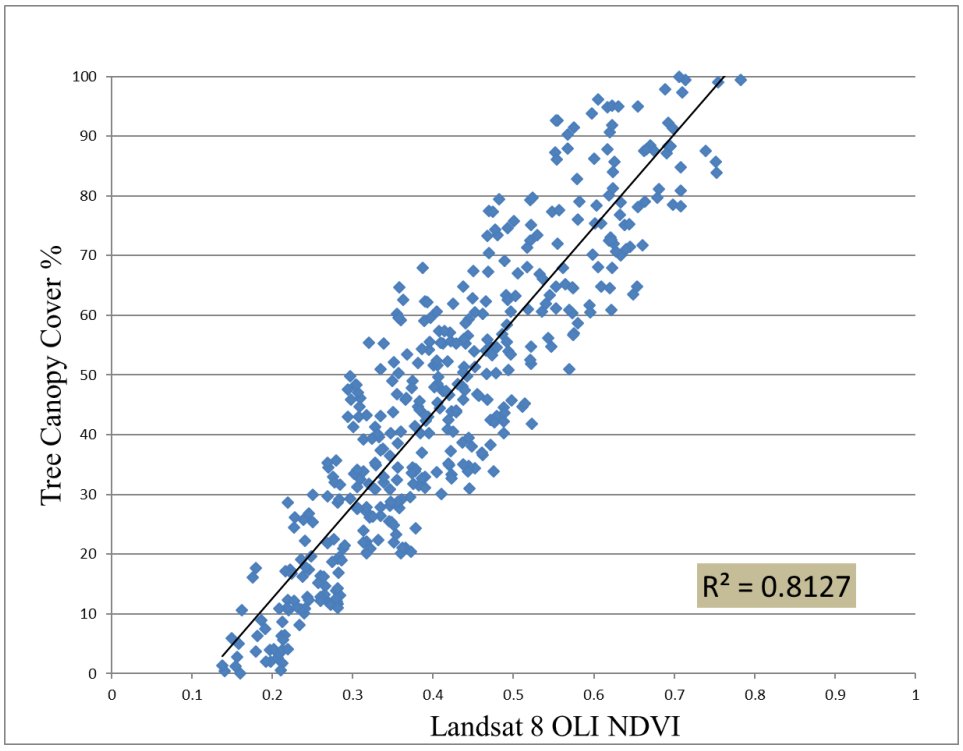

Figure 9: Estimated TCC% versus Landsat 8 NDVI for the training data set (*TCC = 155.48*NDVI - 18.512*). The line represents a linear regression. TCC% Estimations are for the dry season between 2010 and 2015. NDVI from Landsat 8 images in November 2014.

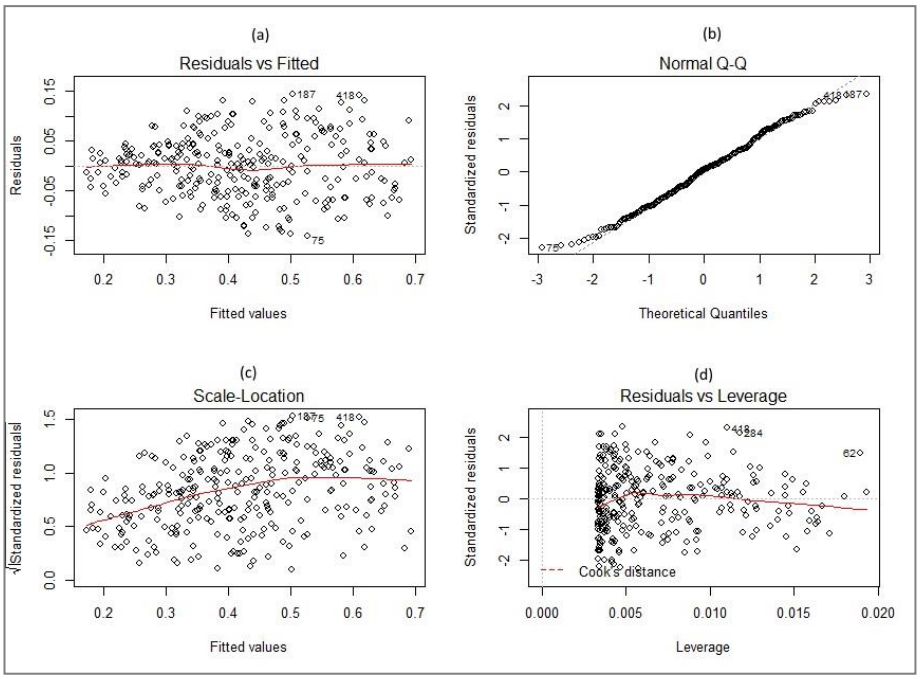

Figure 10: Four residual diagnostic plots to ensure that the linear regression assumption was met. The plots explore a) the existence of a non-linear relationship in the regression, b) the distribution of the residuals, c) the equal variance assumption, and d) the influential or outlier points.

4.2.2 Linear regression using MODIS and GIMMS3g NDVI

Landsat 8 NDVI pixels were averaged and up-scaled to two different spatial resolutions (250m as MODIS NDVI, and 8 km as GIMMS3g NDVI). The up-scaled NDVI was then used to develop two regression models. Equation 5 shows the model for the imagery resampled 250m and Equation 6 for the data resampled to 8 km GIMMSg NDVI):

$$y = 132.2x - 1.4978 \qquad (5)$$

$$y = 94.38x + 22.474 \qquad (6)$$

Where *y* is TCC (%) and *x* is the resampled Landsat 8 NDVI.

NDVI products from MOD13Q1 and GIMMS3g were used to develop two models for estimating TCC in semi-arid Sahel. Equation 7 for MOD13Q1 and equation 8 for GIMMS3g NDVI shows the developed models:

$$y = 178.47x - 2.5843 \quad (7)$$

$$y = 105.64x + 20.646 \quad (8)$$

Where *y* is TCC (%) and *x* is either MOD13Q1 (Equation 7) or GIMMS3g (Equation 8).

Figure 11 demonstrates the relationship between the estimated TCC percentage from Google Earth and NDVI from the motioned above sources. In the case of MOD13Q1 and resampled Landsat 8 regression the results demonstrated a weak correlation. As shown in Figure 11 (A) not more than 51% of the total variance was explained (R^2 = 0.51) and 58% of the variance was explained in Figure 11 (B) where Landsat 8 NDVI was resampled to 250m pixel size. MOD13Q1 dataset NDVI ranged between 0.121 and 0.67 (mean = 0.26) while resampled Landsat 8 NDVI ranged between 0.13 and 081. Figure 11 (C) illustrates the weak correlation (R^2 = 0.10) between estimated TCC and GIMMS3g NDVI as a predictor variable. GIMMS3g NDVI values ranged between 0.108 and 0.46 (mean = 0.269). Figure 11 (D) shows weak correlation also (R^2 = 0.11), yet NDVI values here is in the range between 0.11 and 0.60 (mean = 0.35) in both cases, with the actual medium or coarse resolution and the resampled one. The lack of significant variability in the NDVI values could be regarded as evidence for the weak relationships between TCC and NDVI derived from medium or coarse resolution products.

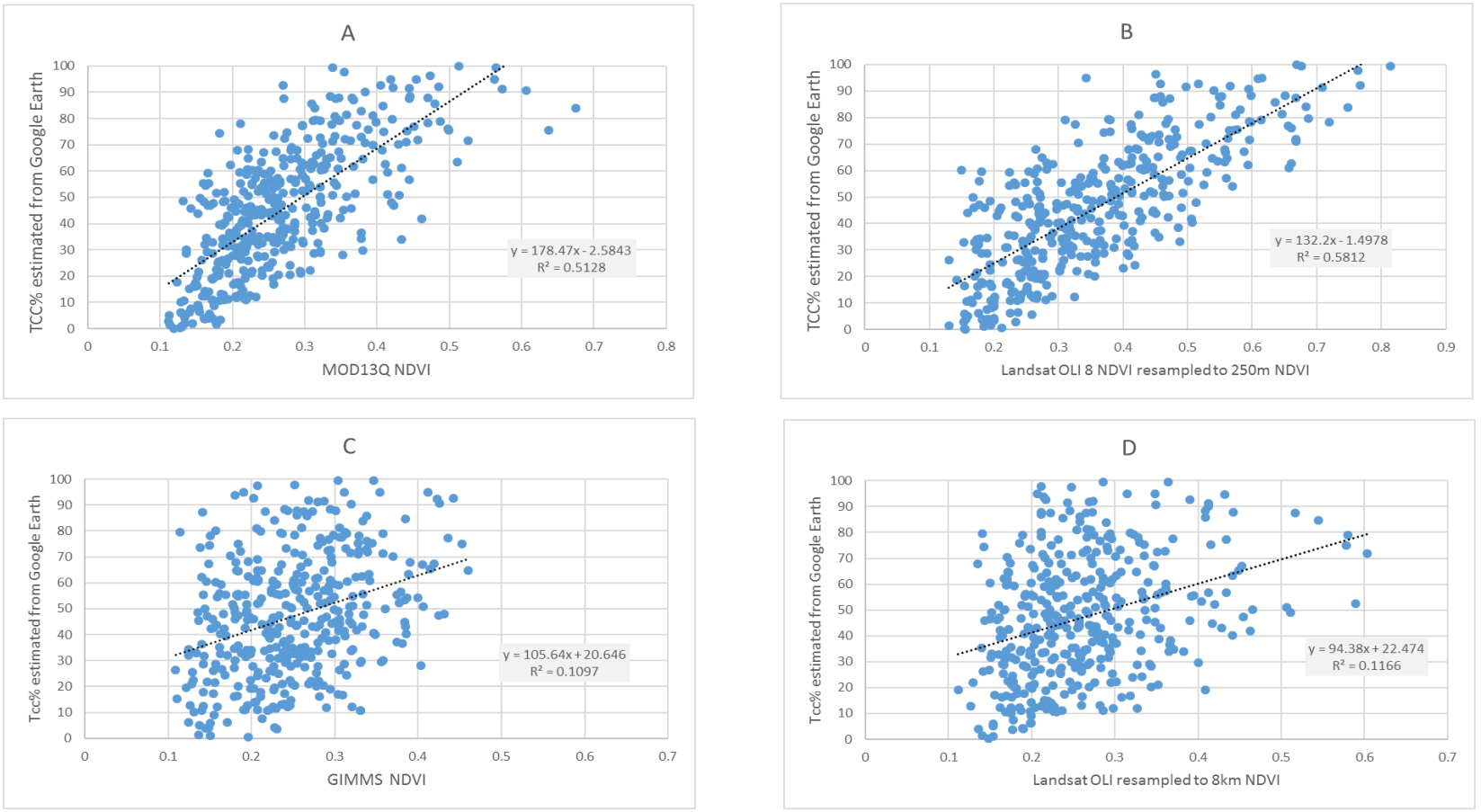

Figure 11: Estimated TCC% versus NDVI from different sources. Plot A), presents MOD13Q1 NDVI with 250 m spatial resolution, acquisition date November 2014. Plot B) illustrates NDVI from Landsat 8 resampled to 250m pixel size. In plot C) GIMMS3g NDVI from December 2013 with an 8-kilometer spatial resolution plot D) Landsat 8 resampled to 8km pixel size in the entire plots the Y axis represent TCC estimated from Google Earth imagery.

4.3 Model validation

The Root Mean Square Error (RMSE, equation 2) between predicted and estimated TCC in the validation dataset, which corresponded to 30% of the data, was 10.70 while the Mean Absolute Error (MAE, equation 3) was 9. Figure 12 A demonstrates the strong correlation (R^2 = 0.83) between estimated and predicted TCC for the validation dataset. Estimated TCC ranged from 0.4% to 99.4% (mean = 43.8%), whereas predicted TCC had a slightly smaller range between 3.3% and 98% (mean = 45.3%). The estimated values overestimated low percentages of TCC and underestimated high percentages. This could be attributed to non-stationarity issues since the Sahel is a very heterogeneous area. A comparison between TCC estimated from Google Earth and TCC percentage predicted using the mentioned above-developed regressions and the developed regressions in equation 5 and equation 6 was held using the same validation dataset. Figure 12 B shows weak correlation (R^2 = 0.59) between tree canopy cover percentage estimated from Google Earth and TCC% predicted using equation 5 based on regression developed using Landsat 8 NDVI data resampled to match the spatial resolution of MOD13Q. and GIMMS (Plot C) While the correlation is weaker between estimated TCC% and the predicted one from equation 6 (Landsat 8 NDVI data resampled to 8 km GIMMSg NDVI)) as shown in figure 12 C

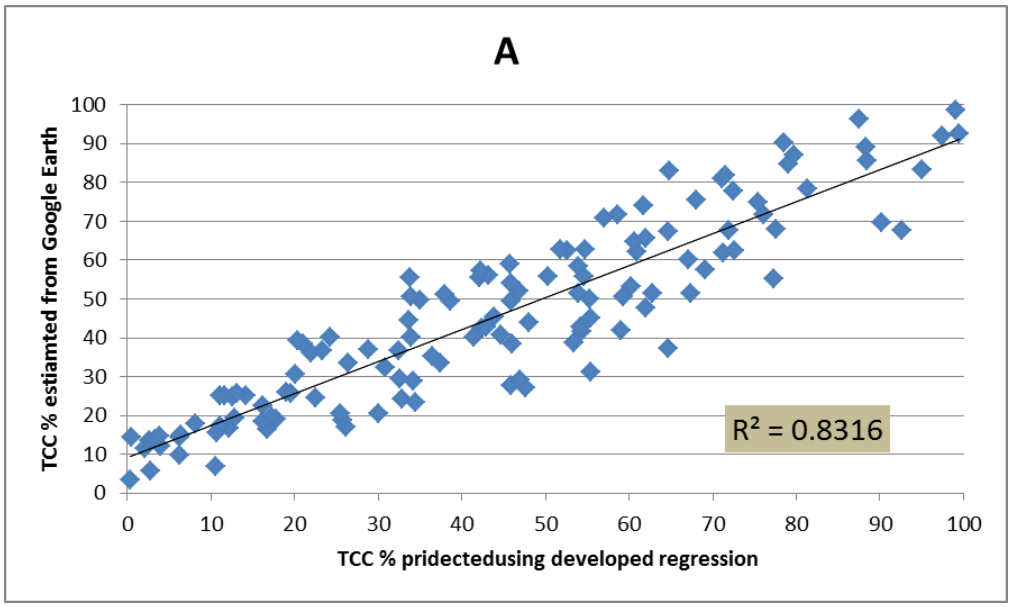

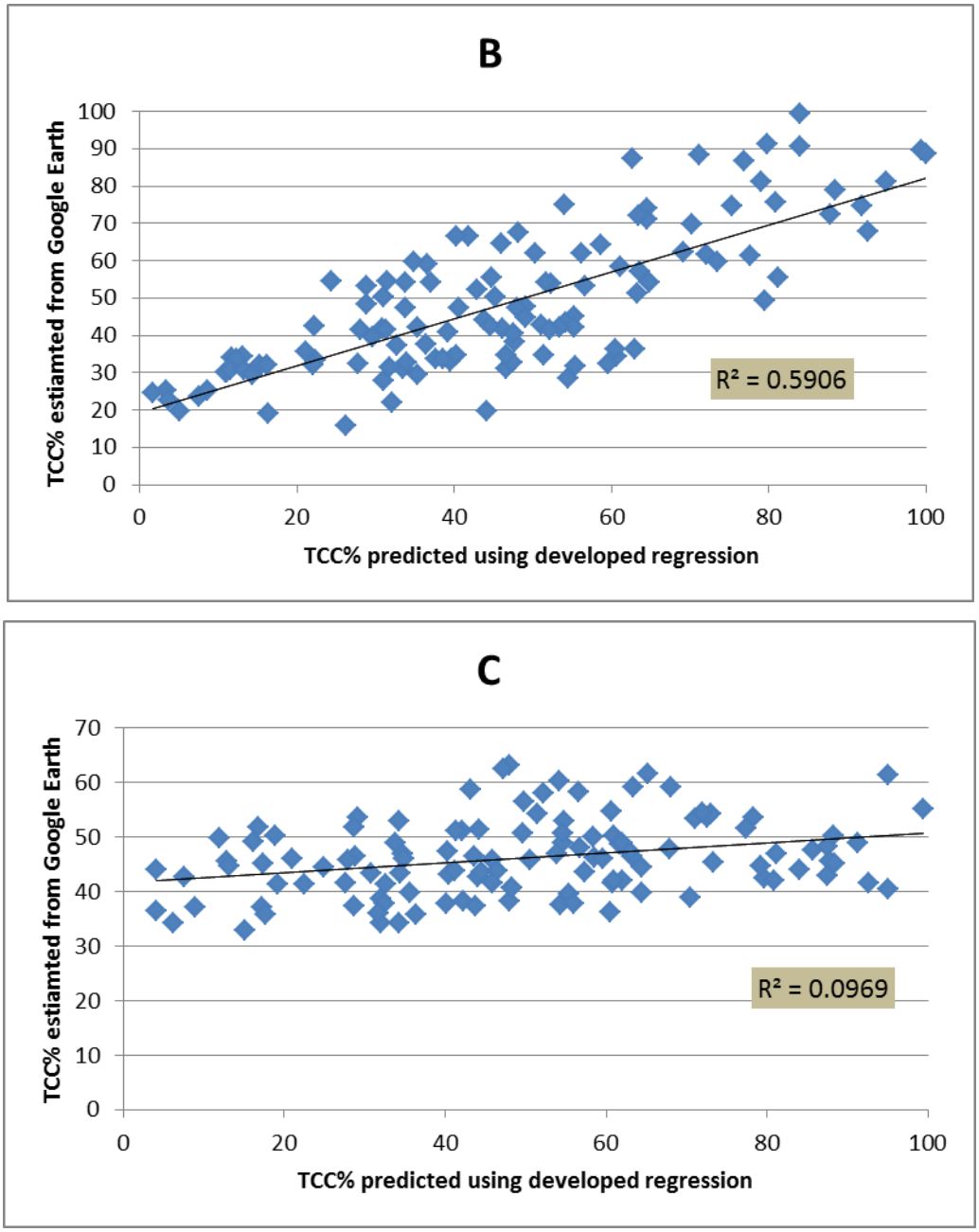

Figure 12: Relationship between estimated and predicted tree canopy cover (TCC). In the X-axes are TCC (%) estimated from Google Earth (30% was kept for validation). While the Y-axes are TCC (%) calculated using the regression developed using 70% of the data. Plot A) shows the TCC (%) predicted from the regression model developed using Landsat 8 data. In plot B and C, the prediction of TCC (%) was based on regression developed using Landsat 8 data resampled to match the spatial resolution of MOD13Q (Plot B) and GIMMS (Plot C).

4.4 Model application

The developed TCC-NDVI regression utilized 50 Landsat 8 scenes from which NDVI was derived. Due to technical limitations (shortage in computational and storage capacities) the regression could not be applied to the entire number of images. Instead, eight scenes from Landsat 8 were mosaicked, and the regression was applied (Figure 13).

Two datasets from MOD13Q1 NDVI acquired in November 2014, and GIMMS3g NDVI from December 2013 covering the study area were used to map the tree canopy cover percentage for the dry season. Figure 14 shows TCC in percentage for the entire Sahel region. The differences in spatial resolution between the two NDVI dataset are observable.

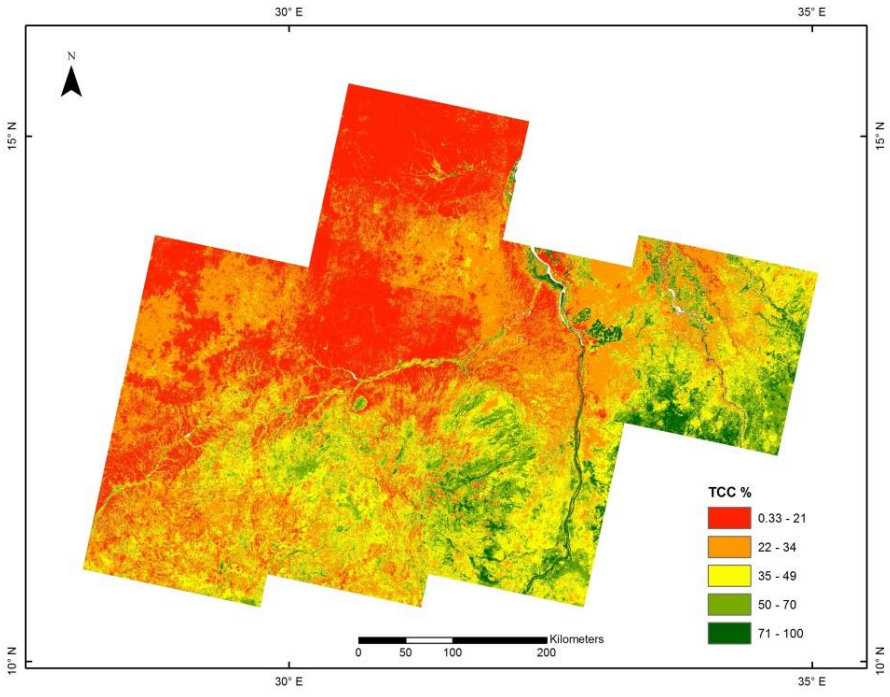

Figure 13: Tree canopy cover percentage in eight mosaicked NDVI images derived from Landsat 8 scenes. The scenes are covering the area in Kordofan region in Sudan. Data acquisition date is November 2014

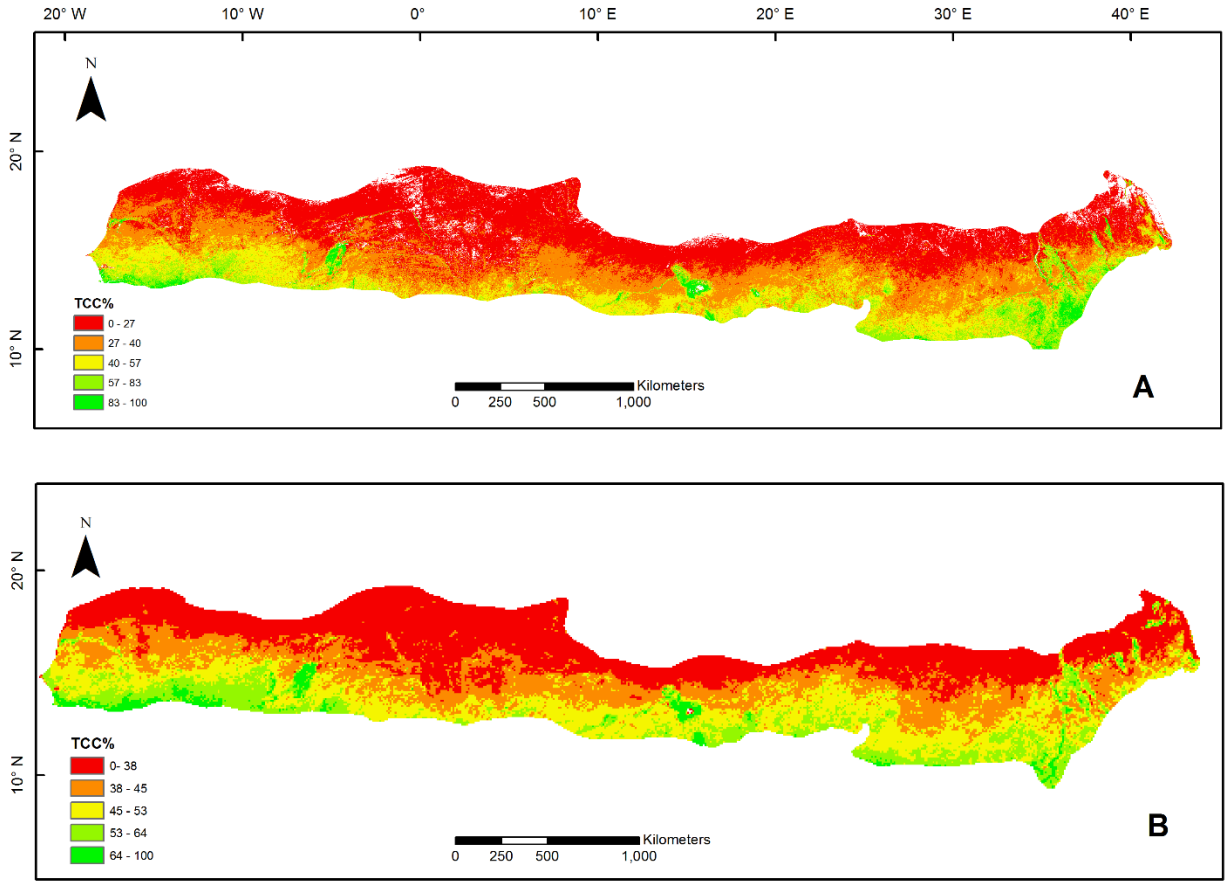

Figure 14: In plot A the developed TCC-NDVI regression (Equation 5) applied to estimate tree canopy cover for entire Sahel using MOD13Q1 NDVI as a proxy. In plot (B) GIMMS3g NDVI used as proxy and equation 6 (developed using Landsat 8 NDVI upscaled to GIMMS 3 spatial resolution) used to estimate TCC (%).

4.5 Comparison between Landsat, MODIS and GIMMS3g NDVI

A comparison between Landsat 8 NDVI data and Landsat NDVI resampled to the spatial resolution of MOD13Q1 and GIMMS3g NDVI was conducted. Figure 15 (A) shows the correlation (R^2 = 0.57) between NDVI from Landsat 8 and NDVI from Landsat 8 resampled to MOD13Q1. In the case of Landsat 8 resampled to GIMMS3g NDVI (Figure 15 (B)), the correlation is weak with not more than 39% of the total variance explained (R^2 = 0.39). In both cases, the lack of significant variability in the NDVI values could be a result of the differences in the spatial resolution between the three sensors beside different spectral configuration.

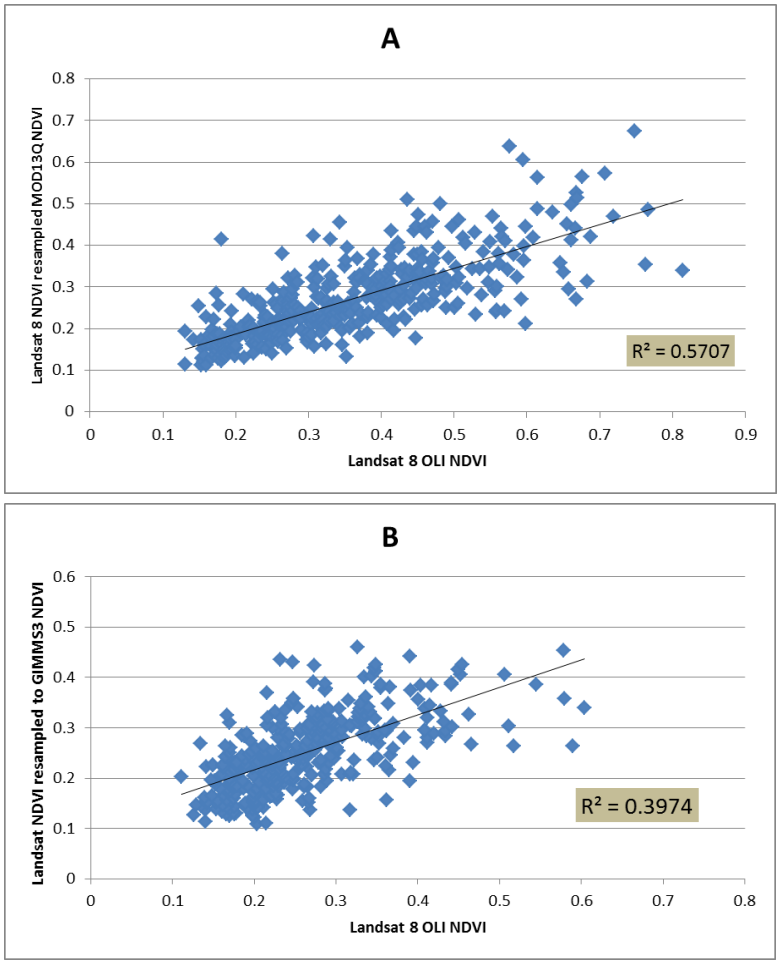

Figure 15: Landsat 8 NDVI versus NDVI resampled to spatial resolution in two different sources. The above plot A), presents Landsat 8 NDVI resampled to the spatial resolution of MOD13Q1 NDVI (250 m), acquisition date November 2014. Plot B) illustrates Landsat 8 NDVI resampled to GIMMS3g NDVI from December 2013 with an 8-kilometer spatial resolution.

Chapter 5: Discussion

5.1 Introduction

This chapter addresses the key findings and limitations. The first section discusses the model development, different spatial resolution effects, reference dataset, and study limitation.

This study developed a linear regression model using Landsat 8 derived NDVI and Google Earth imagery to map tree canopy cover for the Sahel. The results showed that spatially detailed and reasonably accurate maps of TCC can be calculated using the developed linear regression model.

The coefficient of determination (R^2) between Landsat 8 based predictions and the reference data reached 0.80. The accuracy of the developed regression was assessed by splitting the entire dataset into 70% for training and 30% for validation. The correlation between the estimated TCC% and the predicted TCC% was strong ($R^2 > 0.8$) and with low RMSE (RMSE < 10.70). The study also investigated the use of MODIS and GIMMS3g derived NDVI for TCC-NDVI regression development. Landsat 8 NDVI was resampled to the spatial resolution of both GIMMS, and MOD13Q then two regressions were developed and usted to estimate TCC in the whole region in order to compare the outputs.

5.2. Model Development

To estimate tree canopy cover a relationship regression between NDVI as the predictor variable and reference dataset as response variable was developed. Both variables were collected for the dry season which extends from November to May in semi-arid Sahel. The primary assumption was the disappearance of herbaceous vegetation during the dry season meaning the NDVI values will be reflecting the tree vegetation only. However, a study by Horion et al. (2014) investigated the effect of the residual of the dry grass during the dry season on NDVI signal. The study utilized dry season minimum NDVI (NDVImin) values from three NDVI products from varies satellite sensors (GIMMS, MODIS, and Système Pour l'Observation de la Terre (SPOT)-VEGETATION (VGT)). Suggesting that using NDVImin as a proxy to detect tree cover change is not influenced by residuals of dry grass. Irrigated areas and farms irrigated from permanent water source probably were not satisfying the assumption. Future work will include masking this type of land cover. The reference dataset plot size was one hectare to compromise between the cell size in Landsat and MODIS. For each reference data set plot, the corresponding mean NDVI was calculated using Zonal Statistics tool. Mean NDVI was extracted and plotted against TCC percentage. Ordinary linear regression was used to fit the equation between the variables. The developed regression estimated TCC percentage in some area with values under 0% or above 100%. This error in estimation could be because of the nonlinear nature of NDVI. MODIS and GIMMS3g NDVI were used as predictor variables to investigate the effect of the different spatial resolution of NDVI. The results showed a weak correlation between NDVI and the tree cover. The weak correlation could be a result of the aggregation process used in combining the coarse and medium resolution NDVI products. It was also noticed that NDVI from MODIS and GIMMS corresponding to the reference data locations varies in a narrow range. Comparing the results between the regressions developed by Landsat 8, MODIS, and GIMMS showed that Landsat 8 NDVI is more suitable to estimate tree cover in the study area. Landsat 8 imagery comes in large data size (approximately one gigabyte for one scene). NDVI need to be calculated after performing pre-processing and correction on the data. Using Landsat 8 required higher computational power and storage capacity.

To investigate the applicability of applying Landsat 8 developed regression to other NDVI products all the NDVI from the three sources was compared. Results showed a

weak correlation between the three NDVI products from the different sensors. The weak correlation could be a consequence of the variances in spatial resolution between the three sensors. Transferring models developed from Landsat NDVI to MODIS is feasible as stated by Wu et al. (2013). Additionally, various studies suggested there is an agreement between Landsat, MODIS, and GIMMS NDVI products to some extent (Fensholt & Proud 2012; Beck et al. 2011). This is furtherly supported by small differences in the wavelength of the red band and the infrared band used in NDVI products calculation in the three datasets (Figure 16, Table 4).

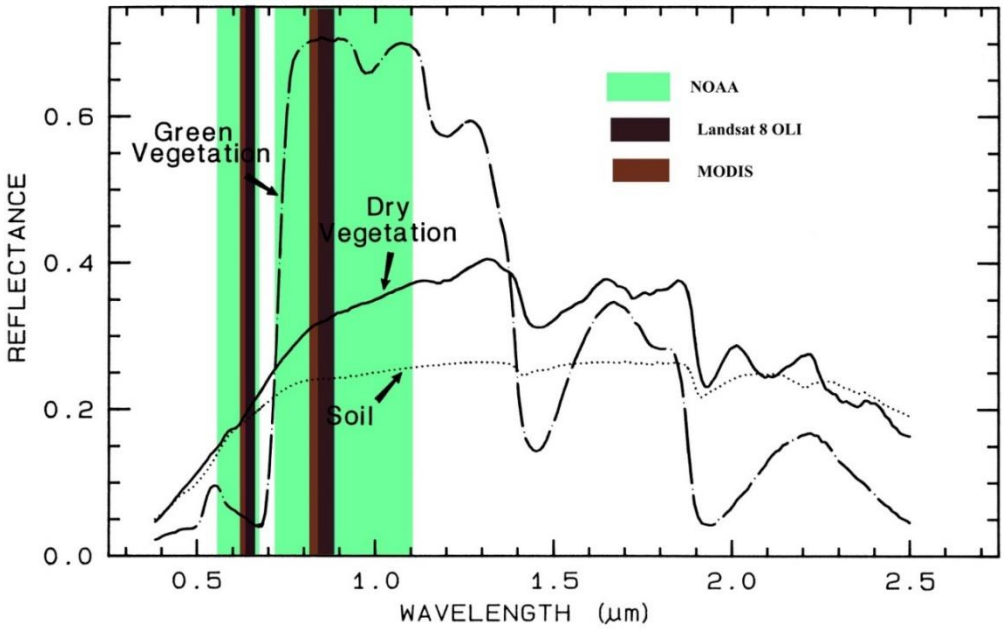

Figure 16: Spectra of green photosynthetic vegetation, dry, non-photosynthetic vegetation, and soil containing montmorillonite. The wavelength of red and infrared bands for NOAA, MODIS, and Landsat 8 OLI sensors is coloured to highlight the small difference between the sensors. The original spectra figure from Clark (2003) which was modified to highlight the satellites of interest.

Table 4: Red and Near-infrared band wavelength for three different sensors.

	Red Band Wavelength (micrometer)	Near-infrared Band Wavelength (micrometer)
NOAA	0.58 – 0.68	0.72 – 1.10
MODIS	0.620 – 0.670	0.841 – 0.876
Landsat 8 OLI	0.64 - 0.67	0.85 - 0.88

The results from the developed method are promising, further research will be required to develop the approach to estimating and mapping particular tree species. Validating the results with field data or data from other authors is essential.

5.3 Reference dataset

This study used Google Earth imagery to derive the reference dataset. Availability of such imagery may be restricted due to low-resolution imagery in parts of the study area. Furthermore; the study utilized the imagery in the dry season (November to May) to avoid the effect of the herbaceous vegetation when estimating the tree canopy cover. It is not the case to acquire imagery from Google Earth satisfying both requirements all the time. One limitation of using Google Earth imagery is in the existence of burned trees in some imagery. These burned trees may lead to errors in the estimation; hence it was estimated as canopy cover in the reference data and has low NDVI values in Landsat8 imagery. All Google Earth imagery plots with burned trees were excluded from the reference dataset. Normal distribution technique was used to collect the reference data set samples location across the region. Proper representation of tree cover per land area was assured. The software used for measuring TCC in each reference data plot provides the possibility of detecting varies color shade and helped to estimate TCC. There is the presence of trees shadow in some reference dataset plots. Enhancing the contrast between the trees and soil was used to detect shadows. Shadow can cause over-estimation of TCC in the plot. Some imagery showed herbaceous vegetation even all the data was collected in the dry season. That could be as result of the location of these areas near to permanent water sources like rivers or lakes which are not dependent on rainfall. Despite the rich combustion of tree species in Sahel this study generalized estimated tree canopy cover for all the species due to the limited knowledge about tree combustion. The results from using Google Earth imagery as reference dataset are promising. However, there is need to improve TCC estimation method to reduce the shadow effect. Google Earth imagery also could be compared with commercial satellite imagery in the case of availability.

Chapter 6: Conclusions

This study mapped tree canopy covers in semi-arid Sahel by developing and validating an empirical TCC-NDVI relationship. Reference dataset from high spatial resolution Google Earth imagery and NDVI derived from Landsat 8 imagery (from the dry season) was used as input in a linear regression (equation 4). Landsat 8 NDVI was also resampled to the spatial resolution of MODIS and GIMMS3g. The resampled NDVI utilized to develop two regressions (equation 5 and 6) in order investigate the effect of different scale (e.g. spatial resolution) in mapping tree canopy cover.

The following conclusions are drawn from this study:

1. Landsat 8 derived NDVI is appropriate for mapping TCC in semi-arid Sahel: the developed regression for TCC resulted in a coefficient of determination (R^2) of 0.80 and a root mean square error (RMSE) of 10 percent.
2. Landsat 8 NDVI is more applicable for TCC-NDVI regression development in comparison to MODIS and GIMMS3g NDVI, and that because of the weak correlation between MODIS/GIMMS3g NDVI and the reference dataset.
3. The approach presented in this study is relatively straightforward and applicable. All the data used in this study is available for public use.

Future research will focus on:

- Evaluating the results of this study with similar studies.
- Developing the approach into more particular tree species.
- Applying the method to a dataset with a different temporal resolution for studying the change in the status of tree canopy cover in Sahel, and using the method for newly available products like Sentinel-2 optical sensor and Advanced Spaceborne Thermal Emission and Reflection Radiometer (ASTER).

References

Abdi, A.M. et al., 2014. The supply and demand of net primary production in the Sahel. *Environmental Research Letters*, 9(9), p.94003. Available at: http://stacks.iop.org/1748-9326/9/i=9/a=094003.

Abrol, D., 2013. *Livelihood Security*, Available at: /citations?view_op=view_citation&continue=/scholar?hl=en&start=20&as_sdt=0,5&scilib=1&scioq=wellness+pollinator&citilm=1&citation_for_view=yHRo6FMAAAAJ:GUJN1xMjMHAC&hl=en&oi=p.

Beck, H.E. et al., 2011. Global evaluation of four AVHRR-NDVI data sets: Intercomparison and assessment against Landsat imagery. *Remote Sensing of Environment*, 115(10), pp.2547–2563. Available at: http://dx.doi.org/10.1016/j.rse.2011.05.012.

Brandt, M. et al., 2014. Modeling Soil and Woody Vegetation in the Senegalese Sahel in the Context of Environmental Change. , 3, pp.770–792. Available at: www.mdpi.com/journal/land.

Brandt, M. et al., 2016. Woody plant cover estimation in drylands from Earth Observation based seasonal metrics. *Remote Sensing of Environment*.

Chavez, P.S., 1988. Chavez PS . An improved dark-object subtraction technique for atmospheric scattering correction of multispectral data . Remote Sensing of Environment An Improved Dark-Object Subtraction Technique for Atmospheric Scattering Correction of Multispectral Data. , 479(February), pp.459–479.

Clark, R.N., 2003. Imaging spectroscopy: Earth and planetary remote sensing with the USGS Tetracorder and expert systems. *Journal of Geophysical Research*, 108(E12), pp.1–2.

Congedo, L., 2014. Semi-Automatic Classification Plugin Documentation. , (September), p.106. Available at: http://fromgistors.blogspot.com.br/p/semi-automatic-classification-plugin.html.

Eklundh, L. & Olsson, L., 2003. Vegetation index trends for the African Sahel 1982–1999. *Geophys. Res. Lett.*, 30(8), p.1430. Available at: http://dx.doi.org/10.1029/2002GL016772.

Fensholt, R. & Proud, S.R., 2012. Evaluation of Earth Observation based global long term vegetation trends - Comparing GIMMS and MODIS global NDVI time series.

Remote Sensing of Environment, 119, pp.131–147. Available at: http://dx.doi.org/10.1016/j.rse.2011.12.015.

Gonzalez, P., Tucker, C.J. & Sy, H., 2012. Tree density and species decline in the African Sahel attributable to climate. *Journal of Arid Environments*.

Herrmann, S.M. & Tappan, G.G., 2013. Vegetation impoverishment despite greening: A case study from central Senegal. *Journal of Arid Environments*.

Hiernaux, P. et al., 2009. Woody plant population dynamics in response to climate changes from 1984 to 2006 in Sahel (Gourma, Mali). *Journal of Hydrology*.

Horion, S. et al., 2014. Using earth observation-based dry season NDVI trends for assessment of changes in tree cover in the Sahel. *International Journal of Remote Sensing*, 35(7), pp.2493–2515. Available at: http://dx.doi.org/10.1080/01431161.2014.883104.

Irons, J.R., Dwyer, J.L. & Barsi, J.A., 2012. The next Landsat satellite: The Landsat Data Continuity Mission. *Remote Sensing of Environment*, 122, pp.11–21. Available at: http://dx.doi.org/10.1016/j.rse.2011.08.026.

Jamali, S. et al., 2014a. Automated mapping of vegetation trends with polynomials using NDVI imagery over the Sahel. *Remote Sensing of Environment*, 141, pp.79–89. Available at: http://dx.doi.org/10.1016/j.rse.2013.10.019.

Jamali, S. et al., 2014b. Automated mapping of vegetation trends with polynomials using NDVI imagery over the Sahel. *Remote Sensing of Environment*, 141, pp.79–89.

Jin, H. & Eklundh, L., 2014. A physically based vegetation index for improved monitoring of plant phenology. *Remote Sensing of Environment*, 152, pp.512–525. Available at: http://dx.doi.org/10.1016/j.rse.2014.07.010.

Karlson, M. et al., 2015. Mapping Tree Canopy Cover and Aboveground Biomass in Sudano-Sahelian Woodlands Using Landsat 8 and Random Forest. *Remote Sensing*, 7(8), pp.10017–10041. Available at: http://www.mdpi.com/2072-4292/7/8/10017/htm.

Karlson, M., 2015. Remote Sensing of Woodland Structure and Composition in the Sudano-Sahelian zone : Application of WorldView-2 and Landsat 8.

Karlson, M. & Ostwald, M., 2016. Remote sensing of vegetation in the Sudano-Sahelian zone: A literature review from 1975 to 2014. *Journal of Arid Environments*, 124(April), pp.257–269. Available at: http://www.sciencedirect.com/science/article/pii/S014019631530046X.

Mbow, C. et al., 2014. Advances in monitoring vegetation and land use dynamics in the Sahel. *Geografisk Tidsskrift-Danish Journal of Geography*, 7223(January 2015), p.8.

Mitchard, E.T.A. et al., 2009. Using satellite radar backscatter to predict above-ground woody biomass: A consistent relationship across four different African landscapes. *Geophysical Research Letters*, 36(23), pp.1–6.

Nicholson, S.E., 2013. The West African Sahel: A Review of Recent Studies on the Rainfall Regime and Its Interannual Variability. *ISRN Meteorology*, 2013(453521), p.32. Available at: http://www.hindawi.com/isrn/meteorology/2013/453521/abs/.

Oduori, S.M. et al., 2011. Assessment of charcoal driven deforestation rates in a fragile rangeland environment in North Eastern Somalia using very high resolution imagery. *Journal of Arid Environments*, 75(11), pp.1173–1181. Available at: http://dx.doi.org/10.1016/j.jaridenv.2011.05.003.

Rasmussen, M.O. et al., 2011. Tree survey and allometric models for tiger bush in northern Senegal and comparison with tree parameters derived from high resolution satellite data. *International Journal of Applied Earth Observation and Geoinformation*, 13(4), pp.517–527. Available at: http://dx.doi.org/10.1016/j.jag.2011.01.007.

Res, C. & Gonzalez, P., 2001. Desertification and a shift of forest species in the West African Sahel. , 17, pp.217–228.

Sankaran, M. et al., Determinants of woody cover in African savannas.

Sendzimir, J., Reij, C.P. & Magnuszewski, P., 2011. Rebuilding Resilience in the Sahel: Regreening in the Maradi and Zinder Regions of Niger. *Ecology and Society*, 16(3), p.8.

Sop, T. & Oldeland, J., 2011. Local perceptions of woody vegetation change in the context of a "Greening Sahel": a case study from Burkina Faso. *Land Degradation & Development*. Available at: citeulike-article-id:9790121%5Cnhttp://onlinelibrary.wiley.com/doi/10.1002/ldr.1144/pdf.

Spiekermann, R., Brandt, M. & Samimi, C., 2014. Woody vegetation and land cover changes in the Sahel of Mali (1967–2011). *International Journal of Applied Earth Observation and Geoinformation*, 34(December), pp.113–121. Available at: http://www.sciencedirect.com/science/article/pii/S0303243414001718.

Thomas M. Lillesand, Ralph W. Kiefer, J.W.C., 1989. *Remote Sensing and Image Interpretation*,

Tucker, C.J., 1979. Red and photographic infrared linear combinations for monitoring vegetation. *Remote Sensing of Environment*, 8(2), pp.127–150.

Vincke, C., Di??dhiou, I. & Grouzis, M., 2010. Long term dynamics and structure of woody vegetation in the Ferlo (Senegal). *Journal of Arid Environments*, 74(2), pp.268–276.

Vrieling, A., De Leeuw, J. & Said, M.Y., 2013. Length of growing period over africa: Variability and trends from 30 years of NDVI time series. *Remote Sensing*, 5(2), pp.982–1000.

Wezel, A., 2005. DECLINE OF WOODY SPECIES IN THE SAHEL. *African Biodiversity*, pp.415–421.

Wu, W., De Pauw, E. & Helldén, U., 2013a. Assessing woody biomass in African tropical savannahs by multiscale remote sensing. *International Journal of Remote Sensing*, 34(13), pp.4525–4549. Available at: http://dx.doi.org/10.1080/01431161.2013.777487.

Wu, W., De Pauw, E. & Helldén, U., 2013b. Assessing woody biomass in African tropical savannahs by multiscale remote sensing. *International Journal of Remote Sensing*, 34(13), pp.4525–4549. Available at: http://www.tandfonline.com/doi/abs/10.1080/01431161.2013.777487.

Institutionen för naturgeografi och ekosystemvetenskap, Lunds Universitet.

Student examensarbete (Seminarieuppsatser). Uppsatserna finns tillgängliga på institutionens geobibliotek, Sölvegatan 12, 223 62 LUND. Serien startade 1985. Hela listan och själva uppsatserna är även tillgängliga på LUP student papers (https://lup.lub.lu.se/student-papers/search/) och via Geobiblioteket (www.geobib.lu.se)

The student thesis reports are available at the Geo-Library, Department of Physical Geography and Ecosystem Science, University of Lund, Sölvegatan 12, S-223 62 Lund, Sweden. Report series started 1985. The complete list and electronic versions are also electronic available at the LUP student papers (https://lup.lub.lu.se/student-papers/search/) and through the Geo-library (www.geobib.lu.se)

372 Andreas Dahlbom (2016) The impact of permafrost degradation on methane fluxes - a field study in Abisko

373 Hanna Modin (2016) Higher temperatures increase nutrient availability in the High Arctic, causing elevated competitive pressure and a decline in *Papaver radicatum*

374 Elsa Lindevall (2016) Assessment of the relationship between the Photochemical Reflectance Index and Light Use Efficiency: A study of its seasonal and diurnal variation in a sub-arctic birch forest, Abisko, Sweden

375 Henrik Hagelin and Matthieu Cluzel (2016) Applying FARSITE and Prometheus on the Västmanland Fire, Sweden (2014): Fire Growth Simulation as a Measure Against Forest Fire Spread – A Model Suitability Study –

376 Pontus Cederholm (2016) Californian Drought: The Processes and Factors Controlling the 2011-2016 Drought and Winter Precipitation in California

377 Johannes Loer (2016) Modelling nitrogen balance in two Southern Swedish spruce plantations

378 Hanna Angel (2016) Water and carbon footprints of mining and producing Cu, Mg and Zn: A comparative study of primary and secondary sources

379 Gusten Brodin (2016) Organic farming's role in adaptation to and mitigation of climate change - an overview of ecological resilience and a model case study

380 Veränika Trollblad (2016) Odling av *Cucumis Sativus* L. med aska från träd som näringstillägg i ett urinbaserat hydroponiskt system

381 Susanne De Bourg (2016) Tillväxteffekter för andra generationens granskog efter tidigare genomförd kalkning

382 Katarina Crafoord (2016) Placering av energiskog i Sverige - en GIS analys

383 Simon Nåfält (2016) Assessing avalanche risk by terrain analysis An experimental GIS-approach to The Avalanche Terrain Exposure Scale (ATES)

384 Vide Hellgren (2016) Asteroid Mining - A Review of Methods and Aspects

385 Tina Truedsson (2016) Hur påverkar snömängd och vindförhållande vattentrycksmätningar vintertid i en sjö på västra Grönland?

386 Chloe Näslund (2016) Prompt Pediatric Care Pediatric patients' estimated travel times to surgically-equipped hospitals in Sweden's Scania County

387 Yufei Wei (2016) Developing a web-based system to visualize vegetation trends by a nonlinear regression algorithm

388 Greta Wistrand (2016) Investigating the potential of object-based image analysis to identify tree avenues in high resolution aerial imagery and lidar data

389 Jessica Ahlgren (2016) Development of a Web Mapping Application for grazing resource information in Kordofan, Sudan, by downloading MODIS data automatically via Python

390 Hanna Axén (2016) Methane flux measurements with low-cost solid state sensors in Kobbefjord, West Greenland

391 Ludvig Forslund (2016) Development of methods for flood analysis and response in a Web-GIS for disaster management

392 Shuzhi Dong (2016) Comparisons between different multi-criteria decision analysis techniques for disease susceptibility mapping

393 Thirze Hermans (2016) Modelling grain surplus/deficit in Cameroon for 2030

394 Stefanos Georganos (2016) Exploring the spatial relationship between NDVI and rainfall in the semi-arid Sahel using geographically weighted regression

395 Julia Kelly (2016) Physiological responses to drought in healthy and stressed trees: a comparison of four species in Oregon, USA

396 Antonín Kusbach (2016) Analysis of Arctic peak-season carbon flux estimations based on four MODIS vegetation products

397 Luana Andreea Simion (2016) Conservation assessments of Văcărești urban wetland in Bucharest (Romania): Land cover and climate changes from 2000 to 2015

398 Elsa Nordén (2016) Comparison between three landscape analysis tools to aid conservation efforts

399 Tudor Buhalău (2016) Detecting clear-cut deforestation using Landsat data: A time series analysis of remote sensing data in Covasna County, Romania between 2005 and 2015

400 Sofia Sjögren (2016) Effective methods for prediction and visualization of contaminated soil volumes in 3D with GIS

401 Jayan Wijesingha (2016) Geometric quality assessment of multi-rotor unmanned aerial vehicle-borne remote sensing products for precision agriculture

402 Jenny Ahlstrand (2016) Effects of altered precipitation regimes on bryophyte carbon dynamics in a Peruvian tropical montane cloud forest

403 Peter Markus (2016) Design and development of a prototype mobile geographical information system for real-time collection and storage of traffic

accident data

404 Christos Bountzouklis (2016) Monitoring of Santorini (Greece) volcano during post-unrest period (2014-2016) with interferometric time series of Sentinel-1A

405 Gea Hallen (2016) Porous asphalt as a method for reducing urban storm water runoff in Lund, Sweden

406 Marcus Rudolf (2016) Spatiotemporal reconstructions of black carbon, organic matter and heavy metals in coastal records of south-west Sweden

407 Sophie Rudbäck (2016) The spatial growth pattern and directional properties of *Dryas octopetala* on Spitsbergen, Svalbard

408 Julia Schütt (2017) Assessment of forcing mechanisms on net community production and dissolved inorganic carbon dynamics in the Southern Ocean using glider data

409 Abdalla Eltayeb A. Mohamed (2016) Mapping tree canopy cover in the semi-arid Sahel using satellite remote sensing and Google Earth imagery

Appendix 1

Table 1: Product specification for DigitalGlobe satellites. Based on data from (http://global.digitalglobe.com/sites/default/files/DigitalGlobe_Core_Imagery_Product_Guide_0.pdf)

	IKONOS	QUICKBIRD	WORLDVIEW-1	WORLDVIEW-2	GEOEYE-1	WORLDVIEW-3
Available Products	Geo, GeoStereo	Basic, Standard, Ortho Ready Standard and AOS	Basic, Basic Stereo, Standard, Ortho Ready Standard/Stereo and AOS	Basic, Basic Stereo, Standard, Ortho Ready Standard/Stereo and AOS	Basic, Basic Stereo, Standard, Ortho Ready Standard/Stereo and AOS	Basic, Basic Stereo, Standard, Ortho Ready Standard/Stereo and AOS
Product Spatial Resolution	80 cm or 1 m Pan 3.2 m or 4 m MS	60 cm Pan 2.4 m MS	50 cm Pan	40 cm, 50 cm Pan 1.6 m, 2.0 m MS	40 cm,50 cm Pan 1.6 m, 2.0 m MS	30 cm[15], 40 cm, 50 cm Pan 1.2 m[15], 1.6 m, 2.0 m MS 7.5 m SWIR[15]
Multispectral Bands	Red, Green, Blue, Near-Infrared 1	Red, Green, Blue, Near-Infrared 1	N/A	Coastal, Blue, Green, Yellow, Red, Red Edge, Near-Infrared 1, and Near-Infrared 2	Red, Green, Blue, Near-Infrared 1	Coastal, Blue, Green, Yellow, Red, Red Edge, Near-Infrared 1, and Near-Infrared 2
Native Accuracy (at nadir on flat terrain)	15 m CE90	23 m CE90	5 m CE90	5 m CE90	5 m CE90	5 m CE90 7.5 m CE90 (SWIR)

Table 2: Product specification for Astrium satellites. Based on data from

(http://www.intelligence-airbusds.com/files/pmedia/public/r12317_9_spot6-7_technical_sheet.pdf)

	Pléiades 1A & 1B constellation	SPOT 6 & 7 constellation
Spatial Resolution	50 cm Panchromatic 1.5 m Multispectral	1.5 m Panchromatic 6 m Multispectral
Multispectral Bands	Panchromatic, Blue, Green, Red, Near-infrared	Panchromatic, Blue, Green, Red And Near-infrared
Native Accuracy (at nadir)	8.5 m CE90	< 18 m CE90

Appendix 2 Information in the table is based on data from (https://earthexplorer.usgs.gov/)

OBJECTID	PATH	ROW	Day	Month	Year	Cloud Cover
1	199	49	11	11	2014	0
2	199	50	11	11	2014	0
3	204	48	17	1	2015	0.01
4	204	49	17	1	2015	0.02
5	204	50	30	11	2014	0.05
6	202	48	19	1	2015	0
7	202	50	4	2	2015	0
8	200	48	18	11	2014	0
9	200	49	18	11	2014	0
10	200	50	18	11	2014	0
11	196	48	6	11	2014	0
12	196	49	6	11	2014	0.08
13	196	50	22	11	2014	0.1
14	194	48	24	11	2014	0
15	194	49	24	11	2014	0.02
16	194	50	24	11	2014	0.03
17	197	49	15	12	2014	0.13
18	197	50	15	12	2014	0.04
19	193	49	1	11	2014	0.01
20	193	50	1	11	2014	0.02
21	189	50	9	11	2014	0.03
23	187	51	21	11	2014	0
25	185	51	9	12	2014	0
26	190	49	28	11	2014	0
27	190	50	28	11	2014	0
28	188	50	14	11	2014	0

OBJECT ID	PATH	ROW	Day	Month	Year	Cloud Cover
29	188	51	14	11	2014	0
31	191	50	19	11	2014	0.01
32	186	51	2	12	2014	0
33	184	51	20	12	2014	0
34	182	50	20	11	2014	0
36	180	51	22	11	2014	0
37	178	50	24	11	2014	0
38	178	51	24	11	2014	0
39	181	50	13	11	2014	0
40	181	51	29	11	2014	0
41	179	51	15	11	2014	0
42	177	51	3	12	2014	0
43	178	52	24	11	2014	0
45	177	52	3	12	2014	0
47	173	51	7	12	2014	0.01
49	173	52	7	12	2014	0
50	171	49	9	12	2014	0
51	174	50	28	11	2014	0
52	174	51	28	11	2014	0
53	174	52	28	11	2014	0
56	172	51	30	11	2014	0
57	170	49	3	1	2015	0.07
59	175	51	19	11	2014	0
60	175	52	5	12	2014	0